

## Automatic histologically-closer classification of skin lesions

Pedro Pedrosa Rebouças Filho<sup>a</sup>, Solon Alves Peixoto<sup>a</sup>, Raul Victor Medeiros da Nóbrega<sup>a</sup>, D. Jude Hemanth<sup>b,\*</sup>, Aldisio Gonçalves Medeiros<sup>a</sup>, Arun Kumar Sangaiah<sup>c</sup>, Victor Hugo C. de Albuquerque<sup>d</sup>

<sup>a</sup> Programa de Pós-Graduação em Ciência da Computação, Instituto Federal de Educação, Ciência e Tecnologia do Ceará, Brazil

<sup>b</sup> ECE Department, Karunya University, India

<sup>c</sup> CSE Department, VIT University, India

<sup>d</sup> Programa de Pós-Graduação em Informática Aplicada, Universidade de Fortaleza, Fortaleza, Ceará, Brazil



### ARTICLE INFO

#### Keywords:

Structural co-occurrence matrix  
Image classification  
Melanoma  
Machine learning

### ABSTRACT

According to the American Cancer Society, melanoma is one of the most common types of cancer in the world. In 2017, approximately 87,110 new cases of skin cancer were diagnosed in the United States alone. A dermatoscope is a tool that captures lesion images with high resolution and is one of the main clinical tools to diagnose, evaluate and monitor this disease. This paper presents a new approach to classify melanoma automatically using structural co-occurrence matrix (SCM) of main frequencies extracted from dermoscopy images. The main advantage of this approach consists in transform the SCM in an adaptive feature extractor improving his power of discrimination using only the image as parameter. The images were collected from the International Skin Imaging Collaboration (ISIC) 2016, 2017 and Pedro Hispano Hospital (PH2) datasets. Specificity (Spe), sensitivity (Sen), positive predictive value, F Score, Harmonic Mean, accuracy (Acc) and area under the curve (AUC) were used to verify the efficiency of the SCM. The results show that the SCM in the frequency domain work automatically, where it obtained better results in comparison with local binary patterns, gray-level co-occurrence matrix and invariant moments of Hu as well as compared with recent works with the same datasets. The results of the proposed approach were: Spe 95.23%, 92.15% and 99.4%, Sen 94.57%, 89.9% and 99.2%, Acc 94.5%, 89.93% and 99%, and AUC 92%, 90% and 99% in ISIC 2016, 2017 and PH2 datasets, respectively.

### 1. Introduction

Annually, millions of patients are diagnosed with skin cancer where approximately 132,000 of these are diagnosed with melanoma. This makes this disease be among the pathologies with the highest overall mortality rates (Song et al., 2018). One-third of all cancer patients has skin cancer and, according to the Skin Cancer Foundation Statistics (Skin Cancer Foundation, 2015), one in five Americans will develop skin cancer during their lifetime.

There are various risk factors that potentiate the appearance of this disease such as: aging, exposure to ultraviolet rays, exposure to harmful chemical elements, and low immunity among others. In many cases, when a patient presents with pathologies that may be associated with these risk factors, this pathology appears as a skin lesion.

One of the most significant challenges related to biomedical engineering is to identify and classify a skin lesion efficiently using

dermoscopy images. Some examples of this type of image are shown in Fig. 1.

Computational vision is one of the main tools being used in the development of new approaches applied to biomedical images where this computing system uses specific patterns in a biomedical image, many of which are already used by the specialist (Rebouças Filho et al., 2017a; Rebouças Filho et al., 2017b; Ramalho et al., 2014a). As all factors not related to the prognosis of the disease are ignored by computer systems, the possibility of error is reduced, and a better clinical diagnosis is offered with greater precision and agility (Rodrigues et al., 2016, 2018; Rebouças Filho et al., 2017c; de Souza et al., 2018).

Nowadays, the pixels of the dermoscopy images provide sufficient information to work in computational environments. Some information is acquired using feature extraction methods based on color and texture, and they have been widely applied to evaluate lesions as in the case of melanomas (Rahman et al., 2016).

\* Corresponding author.

E-mail addresses: [pedrosarf@ifce.edu.br](mailto:pedrosarf@ifce.edu.br) (P.P. Rebouças Filho), [solon.alves@lapisco.ifce.edu.br](mailto:solon.alves@lapisco.ifce.edu.br) (S.A. Peixoto), [raulmedeiros@lapisco.ifce.edu.br](mailto:raulmedeiros@lapisco.ifce.edu.br) (R.V. Medeiros da Nóbrega), [judehemanth@karunya.edu](mailto:judehemanth@karunya.edu) (D.J. Hemanth), [aldisio.medeiros@lapisco.ifce.edu.br](mailto:aldisio.medeiros@lapisco.ifce.edu.br) (A.G. Medeiros), [arunkumarsangaiah@gmail.com](mailto:arunkumarsangaiah@gmail.com) (A.K. Sangaiah), [victor.albuquerque@unifor.br](mailto:victor.albuquerque@unifor.br) (V.H.C. de Albuquerque).

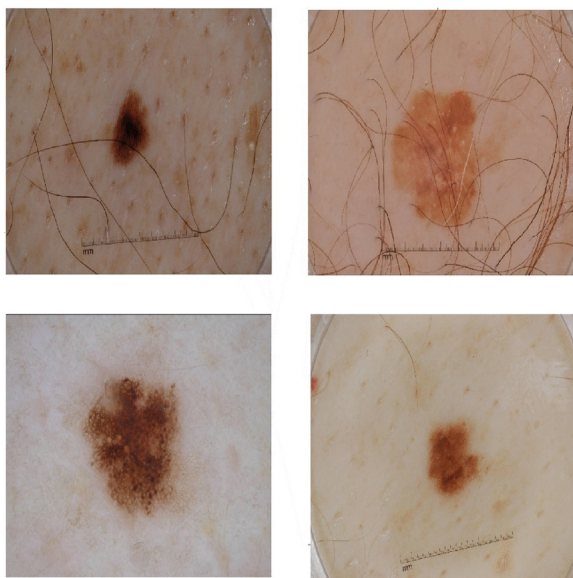


**Fig. 1.** Dermoscopy images of different skin lesions. Some images have a ruler as well as the presence of hairs. The ruler aid in calculating the size of the lesion.

In the paper presented by Kavitha and Suruliandi (2016), color histograms and haralick features were used with support vector machine (SVM) to classify dermoscopy images into melanoma and non-melanoma. The work of Gu et al. (2017) presented an approach based on Mahalanobis distance and constrained graph regularized non-negative matrix factorization to enhance the discriminability of the classification using information of the shape and local color variation.

Other approaches to detect and classify lesions are based on the current technique used by specialists for clinical diagnosis. The aim is to seek the more characteristic data in the images that can be used to facilitate their classification using the asymmetry (A) of the region, the irregularity of its border (B), the variation of colors (C) or intensities of distinct areas and its differential structure (D). The union of these characteristics constitutes the technique known as ABCD (Kavya and Saranya, 2016).

Mete et al. (2016) used the SVM classifier as a tool to compare the types of lesions based on the characteristics extracted by the ABCD standard. A similar approach is presented by Almaraz-Damian et al. (2016) but with the focus in a computer-aided diagnosis (CAD) system for lesion classification.

An important work presented by Waheed et al. (2017) showed that one of the central characteristics used to classify a lesion is the differences in skin tones in the image. In this case, the HSV space for color extraction may be more appropriate due to its similarity to human perception. Kasmi and Mokrani (2016) presented a hair removal technique using the Gabor filter and detection of the edge of the lesion by applying the active geodetic contour.

On the other hand, nowadays the convolutional neural network (CNN) techniques seek to extract the most relevant information from an image and generalize the classification of the injury (Ge et al., 2017; Demyanov et al., 2016).

Yu et al. (2017a) proposed a CNN approach and create a two-stage framework (segmentation and classification) to classify the lesion automatically using limited training data. A hybrid approach was proposed by Yu et al. (2017b) using CNN and Fisher vector for the extraction of the more representative characteristics. Sabbaghi et al. (2016) used bag of features convolutional networks learning with high-quality patterns in dermoscopy images.

Over another perspective, the luminance and color normalization is an important characteristic to be analyzed. Matsunaga et al. (2017) and

Li and Shen (2017) propose a CNN approach but with preprocessing data by using image luminance normalization and superpixels clustering.

One can see that different perspectives of dermoscopy images show that there are patterns that allow the correct classification of a lesion when they are identified through the application of filters that highlight such patterns. In the paper presented by Ramalho et al. (2016), the structural co-occurrence matrix (SCM) was introduced as powerful feature extractor that can use different filters to highlight a specific pattern.

This work proposes an innovation in the configuration of the SCM for classification of skin lesions. Since the lesion can be classified using different patterns (as indicated by the ABCD technique), the proposed method uses the Fourier transform to extract the main frequencies of the image and use that information as the filter input in SCM.

The advantage of this model lies in its ability to evaluate the image automatically and highlight multiple patterns in the lesion using just the information of the image itself. The other presented approaches use feature extractors where they tend to emphasize a specific pattern making some important characteristic not be used.

Since the proposed approach involves multiple patterns recognition simultaneously, this method may be a powerful tool to the use in systems which aid clinical diagnoses. Thus, this work applies different strategies to highlight the main characteristics of dermoscopy images in order to acquire more accurate clinical diagnoses.

This work focuses on:

- The main noises present in dermoscopy images
- Different filters to remove the noises detected
- The lesion structure
- A new approach to classify lesion
- Comparison with other extraction methods
- Comparison with recent results in the literature

This work presents in Section 2 the methodology used to obtain the results including the acquisition of images, preprocessing, feature extraction methods and the classification techniques as also the presentation of the innovation in the SCM configuration. The results are presented and discussed in Section 3 comparing to other configurations and with recent approaches.

## 2. Methodology

### 2.1. Acquiring images

The images used in this work were from the PH2 (Mendonça et al., 2013), ISIC 2016 (Gutman et al., 2016) and ISIC 2017 (Codella et al., 2017) datasets and totaled 3100 dermoscopy images. Except for the PH2 dataset, the images contained in the other datasets have different sizes, a layout of the lesion plus other noises such as marking stickers and rulers. In this study, the melanoma and non-melanoma lesions were classified histologically.

### 2.2. Pre-processing

Some of the dermoscopy images had a bright region as indicated in Fig. 2. This region is due to a gel applied at the moment of the examination. Since the only region of interest is the lesion, the gel and the hairs (noises), in this case, were removed from the image.

After applying the lesion mask, the image pre-processing is finalized by adjusting the contrast between the images. As also perceived by Kawahara et al., the difference in the tone of skin of each person also has a negative influence on the results and therefore is also characterized as a noise. In this case, an average normalization was applied to each image. Pre-processing was performed for image normalization as shown in Fig. 3.



(a) Outline of boundary of the (b) Outline of boundary of the  
glossy region over the lesion glossy region over the lesion

**Fig. 2.** Dermoscopy images with glossy regions indicating the presence of a gel. A yellow outline represents the boundary of the region. (For interpretation of the references to color in this figure legend, the reader is referred to the web version of the article.)

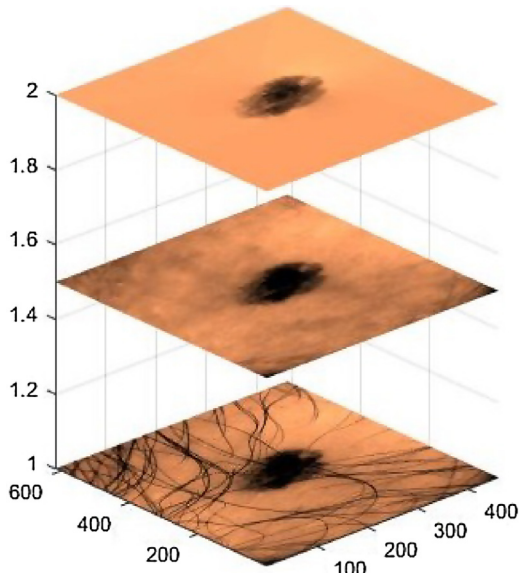


**Fig. 3.** The proposed method for skin normalization. From the bottom, the first step focus on the remotion of the main noises presented in the image as hairs and gel. Second, the shadows of the hairs are removed as well as the skin is normalized to a single tonality. The top image is the result of this preprocessing.

There was a large variation in the sizes of the dermoscopy images in the ISIC 2016 and ISIC 2017 datasets; therefore the size of these images was changed to approximately  $760 \times 570$  pixels. Values were based on the average size of the images in the PH2 dataset. The processing of each image was as follows:

1. Image resizing
2. Transformation to grayscale
3. Noise removal
4. Segmentation mask
5. Contrast adjustment

To adapt the images to the feature extractors used in this work, the resized images were transformed into grayscale and afterwards were processed according to the sequence 1–5, as shown in Fig. 4.

### 2.3. Machine learning techniques

In this work, different machine learning techniques were used to evaluate the efficiency of the feature extractors.

Multi-Layer Perceptron (MLP) is a classification model based on

neural networks. This network is divided into three main layers: Input, Hidden and Output. The Input layer is the starting point for content analysis. Next, in Hidden layer, the activation of subsequent neurons occurs where each binding between neurons has an associated weight. When the impulse finally arrives at the output layer through the activation functions, the output layer returns the result of the operation (Haykin, 2009; Ramalho et al., 2014b; Rebouças Filho et al., 2014).

A hyperplane is used to separate two classes using the SVM from regression analysis where it can trace an “axis” between the classes in such a way that the analysis is as efficient as possible. One of the advantages of this classifier is the robustness in the presence of noise in the data (Vapnik and Vapnik, 1998). An optimization function  $J$  was required to reduce the risk between boundaries of the classification and its presented by:

$$J(w, \xi) = \frac{1}{2} w^T w + c \sum_{i=1}^N \xi_i \quad (1)$$

subject to:

$$y_i [w^T \phi(x_i) + b] \geq 1 - \xi_i, \quad i = 1, \dots, N \quad \xi_i \geq 0, \quad i = 1, \dots, N \quad (2)$$

where  $\omega$  extends for Lagrange multipliers,  $\xi_i$  as slack variable and  $c$  as hyper parameter.

One variation of SVM is the least square SVM (LS SVM). This classifier modifies the original equation proposed by Vapnik (Vapnik and Vapnik, 1998; de Souza et al., 2017). In this case, a substitution is made in the least squares equation while maintaining the efficiency of the classifier as presented in Eq. (3).

$$J(w, b, e) = \frac{1}{2} w^T w + \gamma \frac{1}{2} \sum_{i=1}^N e_i^2 \quad (3)$$

subject to:

$$y_i [w^T \phi(x_i) + b] = 1 - e_i, \quad i = 1, \dots, N \quad (4)$$

In this case,  $e$  is the error unit, and  $\gamma$  indicates the regularization parameter (Samui and Kothari, 2011).

The Minimal Learning Machine (MLM) classification algorithm is a recent machine learning method based on the mapping between points in the input and output spaces. This mapping represents the distance from each point to  $k$  randomly chosen points. In the training process, the distance matrix is multiplied by an estimated distance component  $y$ . This operation generates the distance model for each point. This distance represents a value for the class in which the point belongs. Finally, the test operation is reduced to choosing the shortest distance for the other points. The shortest distance will correspond to the class that will be assigned (de Souza et al., 2015; Marinho et al., 2017, 2018, 2016).

Mesquita et al. (2015) proposed a variation of the MLM where it varies the calculation of the component and uses the  $K$  Nearest Neighbors. The process of testing a new event occurs by choosing the class based on the majority vote of the neighboring  $K$ . In this work, this variation is called MLM-Nearest Neighbors (MLM-NN).

### 2.4. Feature extraction methods

Extraction techniques were developed, from different perspectives, to detect specific attributes and characteristics in an image. These attributes are related to the perception of the specialist and tend to mimic the ABCD approach. The extractors used in this work are mainly based on two types: Moments and Texture, as discussed below.

HU (Hu, 1962) proposed a model to use central moments in the change of scale and rotation of an image from the normalization of each one of them. This technique, known as HU Moments, can describe seven invariant moments of similarity, size, rotation, and translation after the normalized central moments of order  $p$  and  $q$ ,  $\eta_{pq}$ , presented by Eq. (5)

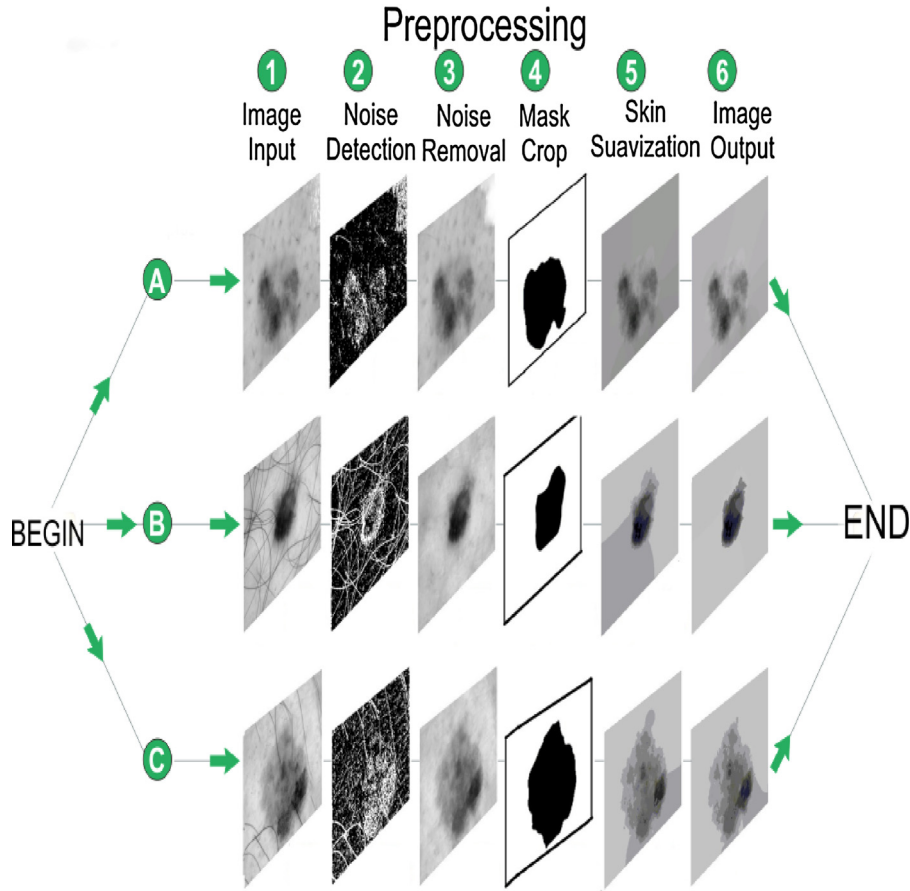


**Fig. 4.** Steps for skin normalization. From the left to right, the hair was removed and the segmentation mask was applied. The final image shows the image with the adjusted contrast.

$$\eta_{pq} = \frac{\mu_{pq}}{\mu_{00}} \quad (5)$$

where

$$\gamma = \frac{p + q}{2}; \quad \forall p + q \geq 2 \quad (6)$$

Then, the seven moments are calculated following by using its result as image attribute. That seven moments are described as

- $I_1 = \eta_{20} + \eta_{02}$
- $I_2 = (\eta_{20} - \eta_{02})^2 + 4\eta_{11}^2$
- $I_3 = (\eta_{30} - 3\eta_{12})^2 + (3\eta_{21} - \eta_{03})^2$
- $I_4 = (\eta_{30} + \eta_{12})^2 + (\eta_{21} + \eta_{03})^2$
- $I_5 = (\eta_{30} - 3\eta_{12})(\eta_{30} + \eta_{12})$   
 $[(\eta_{30} + \eta_{12})^2 - 3(\eta_{21} + \eta_{03})^2] + (3\eta_{21} - \eta_{03})(\eta_{21} + \eta_{03})$   
 $[3(\eta_{30} + \eta_{12})^2 - (\eta_{21} + \eta_{03})^2]$
- $I_6 = (\eta_{20} - \eta_{02})[(\eta_{30} + \eta_{12})^2 - (\eta_{21} + \eta_{03})^2] + 4\eta_{11}(\eta_{30} + \eta_{12})$   
 $(\eta_{21} + \eta_{03})$
- $I_7 = (3\eta_{21} - \eta_{03})(\eta_{30} + \eta_{12})$   
 $[(\eta_{30} + \eta_{12})^2 - 3(\eta_{21} + \eta_{03})^2] - (\eta_{30} - 3\eta_{12})(\eta_{21} + \eta_{03})$   
 $[3(\eta_{30} + \eta_{12})^2 - (\eta_{21} + \eta_{03})^2]$

Haralick et al. (1973) show that using statistical methods in the gray level co-occurrence matrix (GLCM) provides a dependent association between the pixels. From this co-occurrence matrix, it is possible to extract 14 original descriptors described below. For each item in the following equations:

- $p(i, j)$ :  $(i, j)$ -th entry into a standardized gray level matrix  $g(i, j)/N$ ;
- $p_x(i)$ :  $i$ -th entry into a matrix of marginal probability obtained by the

sum of the lines of  $p(i, j)$ ,  $\sum_{j=1}^L p(i, j)$ ;

- $L$ : Number of gray levels in quantized image;
- $\Sigma_i$  and  $\Sigma_j$ : simplified form of  $\sum_{i=1}^L$  and  $\sum_{j=1}^L$ , respectively;
- $p_{x+y}(k) = \sum_{i=1}^L \sum_{j=1, i+j=k}^L p(i, j)$  for  $k = 2, 3, \dots, 2L$ ;
- $p_{x-y}(k) = \sum_{i=1}^L \sum_{j=1, |i-j|=k}^L p(i, j)$  for  $k = 0, 1, \dots, 2L - 1$ .

- Angular second moment:

$$f_1 = \sum_i \sum_j [p(i, j)]^2. \quad (7)$$

- Contrast:

$$f_2 = \sum_{k=0}^{L-1} k^2 [p_{x-y}(k)]. \quad (8)$$

- Correlation:

$$f_3 = \frac{\sum_i \sum_j (i, j)p(i, j) - \mu_x \mu_y}{\sigma_x \sigma_y}, \quad (9)$$

where  $\mu_x$ ,  $\mu_y$ ,  $\sigma_x$  and  $\sigma_y$  are mean and standard deviation of  $p_x$  and  $p_y$ .

- Sum of squares: variance

$$f_4 = \sum_i \sum_j (i - \mu)^2 p(i, j). \quad (10)$$

- Inverse difference moment:

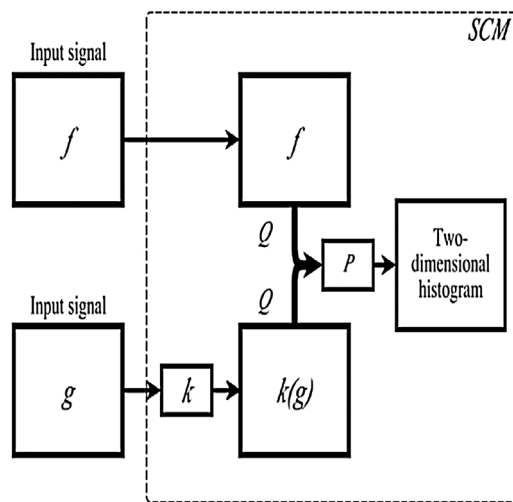


**Fig. 5.** Generic SCM model for two input signals. This signal will be filtered by applying a function  $K$ . Then the SCM (two dimensional histogram) is created using both original and the modified signal  $k(g)$ .

$$f_5 = \sum_i \sum_j \frac{1}{1 + (i + j)^2} p(i, j) \quad (11)$$

- Sum average:

$$f_6 = \sum_{i=2}^{2L} i p_{x+y}(i). \quad (12)$$

- Sum variance:

$$f_7 = \sum_{i=2}^{2L} (i - f_6)^2 p_{x+y}(i). \quad (13)$$

- Sum entropy:

$$f_8 = - \sum_{i=2}^{2L} p_{x+y}(i) \log[p_{x+y}(i)]. \quad (14)$$

- Entropy:

$$f_9 = - \sum_i \sum_j p(i, j) \log[p(i, j)]. \quad (15)$$

- Difference variance:

$$f_{10} = \text{variance of } p_{x+y}. \quad (16)$$

- Difference entropy:

$$f_{11} = - \sum_{i=0}^{L-1} p_{x-y} \log[p_{x-y}(i)]. \quad (17)$$

- Info. measure of correlation (1 and 2):

$$f_{12} = \frac{\text{HXY} - \text{HXY1}}{\max[\text{HX}, \text{HY}]}, \quad (18)$$

$$f_{13} = 1 - \exp[-2.0(\text{HXY2} - \text{HXY})]^{1/2}, \quad (19)$$

where:

-  $\text{HXY} = - \sum_i \sum_j p(i, j) \log[p(i, j)];$

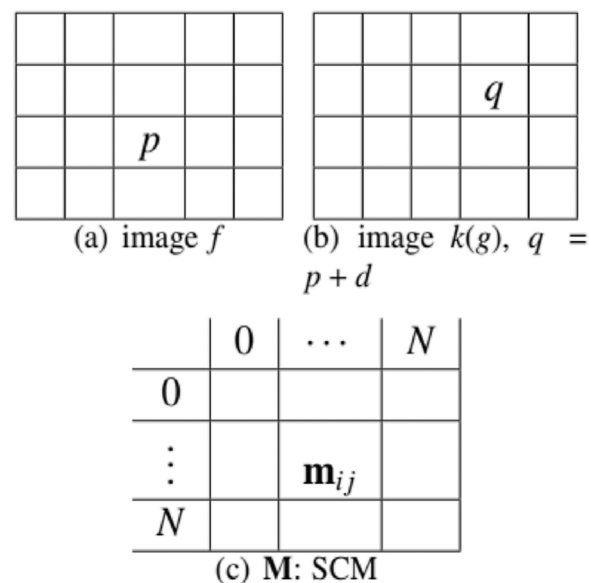


**Fig. 6.** SCM creation process. The first image (a) is related to the second image (b). In this case, the process mimics the GLCM using a distance between the position of pixel  $p$  and the position of pixel  $q$  using a selected angle. (c) SCM created.

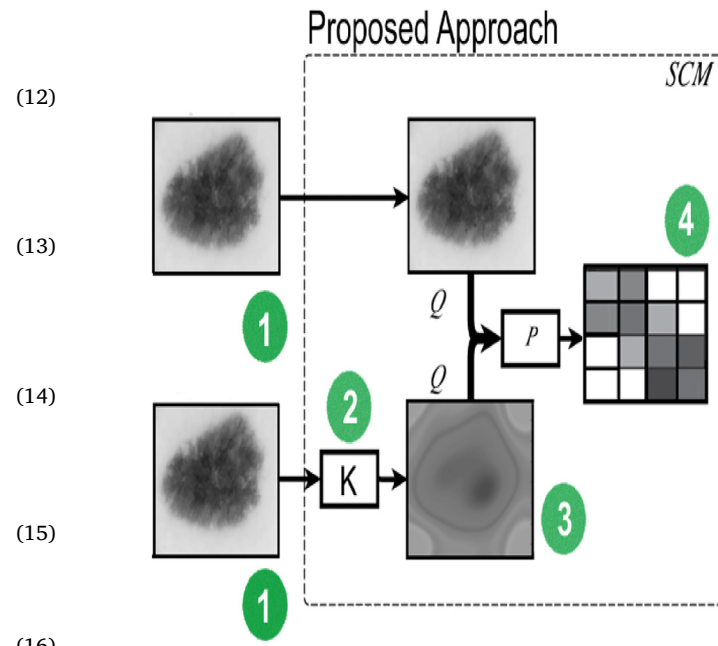


**Fig. 7.** Example of the proposed approach. Step 1 indicates the lesion as input image following by using the main frequencies extracted from Fourier transform as  $K$  function, in step 2. Then the SCM is created in step 3 by using the original and the modified image. Step 4 shows the generated scm.

-  $\text{HX}$  and  $\text{HY}$  are entropy of  $p_x$  e  $p_y$ ;

-  $\text{HXY1} = - \sum_i \sum_j p(i, j) \log[p_x(i)p_y(j)];$

-  $\text{HXY2} = - \sum_i \sum_j p_x(i)p_y(j) \log[p_x(i)p_y(j)].$

- Max. correlation coefficient

$$f_{14} = (\text{Square root of largest eigenvalue } \mathbf{Q})^{1/2}, \quad (20)$$

where:

$$\mathbf{Q} = \sum_k \frac{p(i, k)p(j, k)}{p_x(i)p_y(k)}. \quad (21)$$

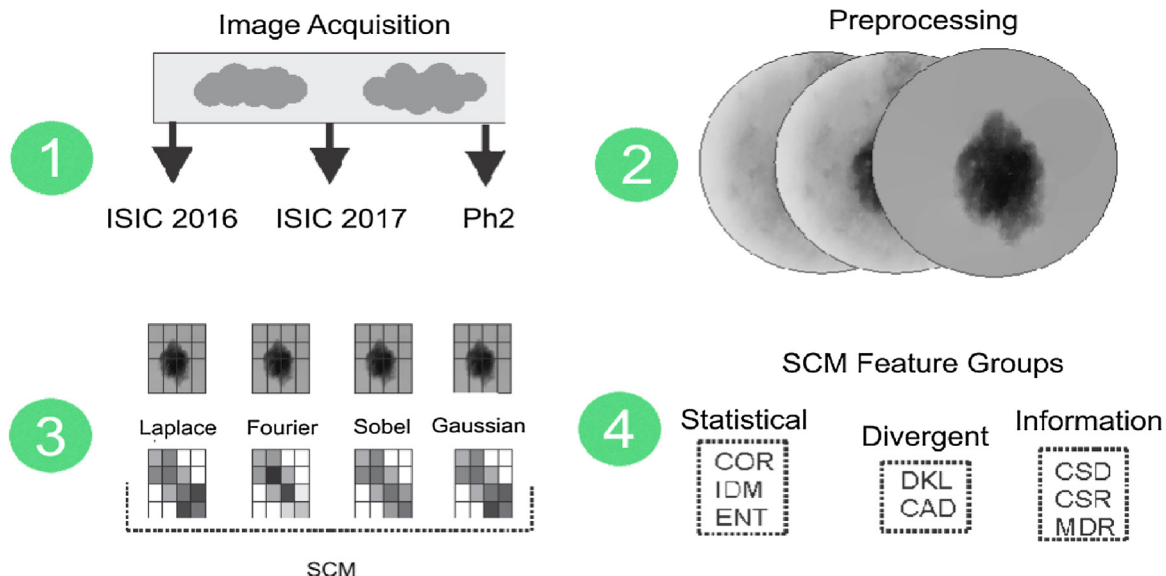


**Fig. 8.** Proposed methodology. The step 1 initially stored the databases followed by the preprocessing as indicated in step 2. In the sequence, the step 3 shows the creation of the SCM matrix for different filters and finally, in the step 4, the extraction of the attributes.

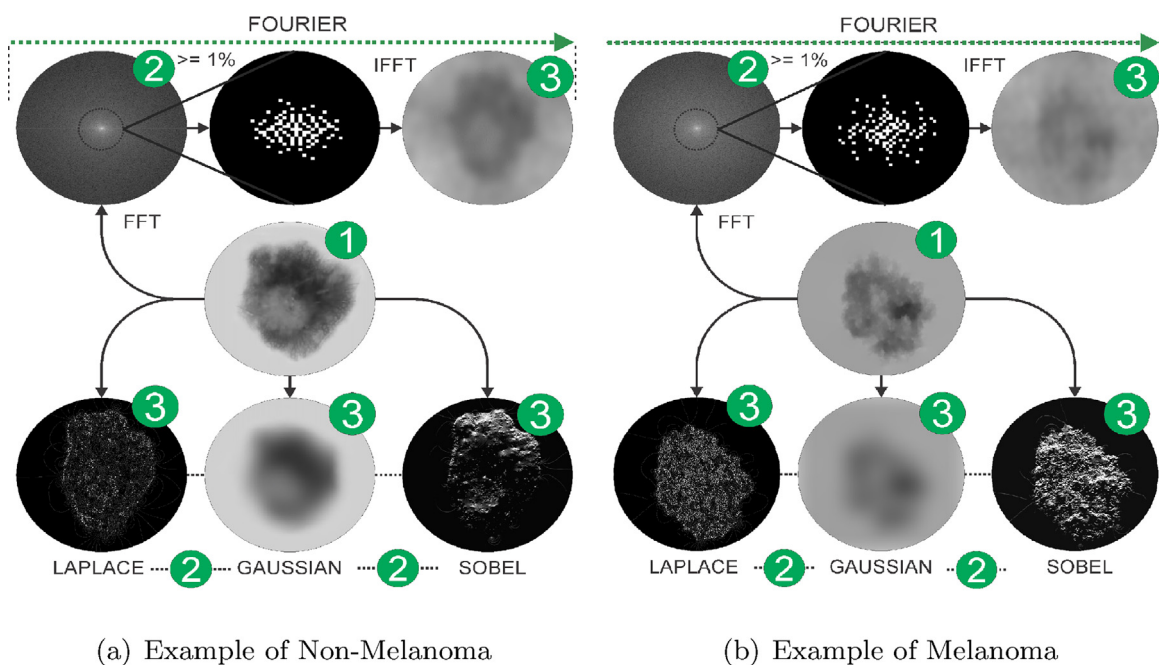


**Fig. 9.** Application of SCM with different Filters. On the left, dermoscopy of a lesion classified as Non-Melanoma and, on the right, Melanoma. Following the steps as described in Fig. 7, (1) input image ( $g$ ), (2) applied filter ( $k$ ), (3) output image  $k(g)$ .

Using the texture analysis of an image, Ojala et al. (1994) formulated a feature extractor called Local Binary Patterns (LBP). This extractor analyzes the neighborhood of a pixel by classifying each pixel in a binary form. The labeling of each neighbor is made from the value of the central pixel where it is seen as a threshold. Thus, pixels above this value will be represented by 1 or 0. Then a code is generated by the 8-bit representation that is the value of the texture. The present work applied a uniform pattern of this extractor (LBP) to present 59 unique attributes (Neto et al., 2015; Rebouças Filho et al., 2017d; Holanda et al., 2018).

## 2.5. Structural co-occurrence matrix

This work proposes a new and efficient approach for extracting

features in dermoscopy images. This approach is based on the SCM designed by Ramalho et al. (2016).

The SCM helps to improve the identification of structures of an object by applying a highlighting function  $k$  to it, as shown in Fig. 5. This function is defined according to the need of each problem and when it is associated with images,  $k$  is a filter where it will highlight the most important characteristics of that image (Ramalho et al., 2016).

The SCM uses the original image and the filtered image where each pixel of the original image will be related to a pixel of the filtered image according to some neighborhood criterion. Fig. 6 illustrates the behavior and the creation of the structural co-occurrence matrix.

Finally, this matrix is added to its transpose and, therefore, the symmetric matrix is generated and this the matrix from which the attributes of the SCM will be extracted.

**Table 1**

Result of classification of dermoscopy images from the Ph2 dataset using LBP, GLCM, and HU considering the specificity (Spe), sensibility (Sen), positive predictive value (Ppv), F score, harmonic mean (Hm) and accuracy (Acc) as evaluation metrics.

Feature	Classifier	Setup	Spe(%)	Sen(%)	Ppv(%)	F score(%)	Hm(%)	Acc(%)
LBP	mlm	cityblock	98.8 ± 0.02	98.33 ± 0.03	98.61 ± 0.02	98.34 ± 0.03	98.46 ± 0.03	98.33 ± 0.03
		euclidean	98.8 ± 0.02	98.33 ± 0.03	98.61 ± 0.02	98.34 ± 0.03	98.46 ± 0.03	98.33 ± 0.03
		mahalanobis	9.62 ± 0.3	50.83 ± 0.02	99.3 ± 0.02	66.7 ± 0	7.05 ± 0.22	50.83 ± 0.02
		mahalanobis	9.62 ± 0.3	50.83 ± 0.02	99.3 ± 0.02	66.7 ± 0	7.05 ± 0.22	50.83 ± 0.02
	mlmNN	cityblock	98.8 ± 0.02	98.33 ± 0.03	98.61 ± 0.02	98.34 ± 0.03	98.46 ± 0.03	98.33 ± 0.03
		euclidean	98.8 ± 0.02	98.33 ± 0.03	98.61 ± 0.02	98.34 ± 0.03	98.46 ± 0.03	98.33 ± 0.03
	svm	Linear	97.97 ± 0.01	96.66 ± 0.02	97.5 ± 0.02	96.72 ± 0.02	97.03 ± 0.02	96.66 ± 0.02
		RBF	97.97 ± 0.01	96.66 ± 0.02	97.5 ± 0.02	96.72 ± 0.02	97.03 ± 0.02	96.66 ± 0.02
	mlp		97.73 ± 0.03	95.83 ± 0.07	97.08 ± 0.04	95.93 ± 0.06	96.37 ± 0.06	95.83 ± 0.07
		RBF	95.83 ± 0.02	94.16 ± 0.04	95.13 ± 0.03	94.2 ± 0.03	94.61 ± 0.03	94.16 ± 0.04
GLCM	lssvm	linear	94.28 ± 0.03	90 ± 0.06	92.77 ± 0.04	90.21 ± 0.06	91.2 ± 0.05	90 ± 0.06
		bayes	0 ± 0	50 ± 0	100 ± 0	66.66 ± 0	0 ± 0	50 ± 0
	MLM-NN	mahalanobis	95.71 ± 0.03	90.83 ± 0.09	94.3 ± 0.05	91.23 ± 0.09	92.26 ± 0.08	90.83 ± 0.09
		cityblock	91.07 ± 0.07	89.16 ± 0.07	90.41 ± 0.07	89.26 ± 0.07	89.7 ± 0.07	89.16 ± 0.07
		euclidean	92.16 ± 0.06	87.5 ± 0.08	90.69 ± 0.06	87.8 ± 0.07	88.84 ± 0.07	87.5 ± 0.08
		Euclidean	92.16 ± 0.06	87.5 ± 0.08	90.69 ± 0.06	87.8 ± 0.07	88.84 ± 0.07	87.5 ± 0.08
	MLM	mahalanobis	95.71 ± 0.03	90.83 ± 0.09	94.3 ± 0.05	91.23 ± 0.09	92.26 ± 0.08	90.83 ± 0.09
		Cityblock	91.07 ± 0.07	89.16 ± 0.07	90.41 ± 0.07	89.26 ± 0.07	89.7 ± 0.07	89.16 ± 0.07
	mlp		90.95 ± 0.05	78.33 ± 0.08	88.05 ± 0.04	79.79 ± 0.07	82.15 ± 0.06	78.33 ± 0.08
		rbf	91.69 ± 0.07	88.33 ± 0.08	90.55 ± 0.07	88.51 ± 0.07	89.28 ± 0.07	88.33 ± 0.08
	svm	linear	89.96 ± 0.09	84.16 ± 0.1	88.47 ± 0.08	84.64 ± 0.1	85.88 ± 0.09	84.16 ± 0.1
		rbf	94.04 ± 0.03	88.33 ± 0.08	92.22 ± 0.04	88.7 ± 0.07	89.97 ± 0.06	88.33 ± 0.08
	lssvm	linear	91.45 ± 0.07	85 ± 0.1	89.72 ± 0.07	85.57 ± 0.09	86.91 ± 0.08	85 ± 0.1
		bayes	90.47 ± 0.06	87.5 ± 0.08	89.58 ± 0.06	87.72 ± 0.07	88.36 ± 0.07	87.5 ± 0.08
HU	svm	linear	91.9 ± 0.03	83.33 ± 0.07	89.44 ± 0.04	84.02 ± 0.07	85.84 ± 0.06	83.33 ± 0.07
		rbf	66.1 ± 0.45	62.5 ± 0.13	93.75 ± 0.04	71.13 ± 0.07	53.4 ± 0.37	62.5 ± 0.13
	lssvm	linear	92.14 ± 0.06	79.16 ± 0.11	89.3 ± 0.06	80.73 ± 0.1	83.3 ± 0.08	80.83 ± 0.09
		RBF	89.02 ± 0.07	80.83 ± 0.09	87.08 ± 0.07	81.71 ± 0.08	83.11 ± 0.09	79.16 ± 0.11
	mlp		77.74 ± 0.3	72.5 ± 0.16	86.25 ± 0.13	75.95 ± 0.13	70.71 ± 0.27	72.5 ± 0.16
		euclidean	67.97 ± 0.13	66.66 ± 0.11	68.61 ± 0.11	67 ± 0.11	67.08 ± 0.12	66.66 ± 0.11
	mlm	mahalanobis	67.97 ± 0.13	66.66 ± 0.11	68.61 ± 0.11	67 ± 0.11	67.08 ± 0.12	66.66 ± 0.11
		cityblock	70.15 ± 0.11	68.33 ± 0.1	70.83 ± 0.1	68.78 ± 0.09	68.95 ± 0.1	68.33 ± 0.1
	mlmNN	cityblock	70.15 ± 0.11	68.33 ± 0.1	70.83 ± 0.1	68.78 ± 0.09	68.95 ± 0.1	68.33 ± 0.1
		euclidean	67.97 ± 0.13	66.66 ± 0.11	68.61 ± 0.11	67 ± 0.11	67.08 ± 0.12	66.66 ± 0.11
		mahalanobis	67.97 ± 0.13	66.66 ± 0.11	68.61 ± 0.11	67 ± 0.11	67.08 ± 0.12	66.66 ± 0.11
	bayes		48.1 ± 0.5	54.16 ± 0.04	96.52 ± 0.03	66.87 ± 0	35.29 ± 0.37	54.16 ± 0.04

This work proposes an innovation in the SCM configuration modifying the input image in function of  $k$  in the frequency domain using the Fourier transform. The resulting image  $K(g)$  shows the main structural characteristics of the image, thus implying a more effective enhancement by SCM. An example of this approach is present in Fig. 7.

This technique consists in extracting, from the magnitude spectrum, only the frequencies that have an intensity of at least 1% of the main DC component and, therefore, only the most important structures in the image will remain in the spectrum (Fisher et al., 1994). In this case, the function  $k$  behaves, for each magnitude, according to the following equation:

$$k(x, y) = \begin{cases} m(x, y), & m(x, y) \geq DC/100 \\ 0, & \text{otherwise,} \end{cases} \quad (22)$$

where  $m(x, y)$  is the magnitude of the component analyzed at the point  $(x, y)$  of the spectrum. The function  $k$  in the frequency domain obtains a

dynamic behavior that fits according to the main structures present in the image, and is, therefore, a powerful function capable of working in different bands simultaneously.

The SCM finally receives  $K(g)$ , generated from the inverse transform of the frequency domain, into the spatial domain and continue the process of the matrix creation. The SCM extract from its matrix 9 attributes divided in 3 groups: statistical, divergent and information. In the statistical group are included the correlation (COR), inverse difference moment (IDM), entropy (ENT). The divergent group presents the divergence of Kullback & Leibler (DKL) and complementary absolute difference (CAD). The information group presents Chi-square distance (CSD), Chi-square distance ratio (CSR) and mean absolute difference ratio (MDR) (Ramalho et al., 2016).

## 2.6. Metrics

The comparison between the results of the SCM with other methods

**Table 2**

Result of classification of dermoscopy images from the Ph2 dataset using SCM considering the specificity (Spe), sensibility (Sen), positive predictive value (Ppv), F score, harmonic mean (Hm) and accuracy (Acc) as evaluation metrics.

Filter	Classifier	Setup	Spe(%)	Sen(%)	Ppv(%)	F score(%)	Hm(%)	Acc(%)
Fourier	SVM	Linear	99.4 ± 0.03	99.16 ± 0.05	99.3 ± 0.04	99.17 ± 0.05	99.23 ± 0.05	99.16 ± 0.05
		RBF	99.4 ± 0.03	99.16 ± 0.05	99.3 ± 0.04	99.17 ± 0.05	99.23 ± 0.05	99.16 ± 0.05
	LSSVM	Linear	95.71 ± 0.03	91.66 ± 0.08	94.44 ± 0.05	91.94 ± 0.08	92.83 ± 0.07	91.66 ± 0.08
		RBF	96.78 ± 0.03	95 ± 0.05	96.11 ± 0.04	95.07 ± 0.05	95.49 ± 0.05	95 ± 0.05
		Cityblock	96.19 ± 0.03	94.16 ± 0.05	95.41 ± 0.04	94.24 ± 0.05	94.72 ± 0.04	94.16 ± 0.05
	MLM	Euclidean	96.19 ± 0.03	94.16 ± 0.05	95.41 ± 0.04	94.24 ± 0.05	94.72 ± 0.04	94.16 ± 0.05
		Mahalanobis	96.19 ± 0.03	94.16 ± 0.05	95.41 ± 0.04	94.24 ± 0.05	94.72 ± 0.04	94.16 ± 0.05
	MLM-NN	Cityblock	96.19 ± 0.03	94.16 ± 0.05	95.41 ± 0.04	94.24 ± 0.05	94.72 ± 0.04	94.16 ± 0.05
		Euclidean	96.19 ± 0.03	94.16 ± 0.05	95.41 ± 0.04	94.24 ± 0.05	94.72 ± 0.04	94.16 ± 0.05
	MLP	Mahalanobis	96.19 ± 0.03	94.16 ± 0.05	95.41 ± 0.04	94.24 ± 0.05	94.72 ± 0.04	94.16 ± 0.05
		Bayes	97.38 ± 0.03	95.83 ± 0.05	96.8 ± 0.04	95.89 ± 0.05	96.26 ± 0.05	95.83 ± 0.05
Gaussian	Bayes	Bayes	97.97 ± 0.03	95.83 ± 0.08	97.36 ± 0.04	96.01 ± 0.07	96.46 ± 0.06	95.83 ± 0.08
		Linear	78.36 ± 0.12	70.83 ± 0.09	77.91 ± 0.1	71.97 ± 0.09	73.24 ± 0.1	70.83 ± 0.09
	LSSVM	Linear	83.77 ± 0.1	75 ± 0.08	82.22 ± 0.08	76.18 ± 0.07	77.71 ± 0.07	75 ± 0.08
		RBF	75.78 ± 0.14	69.16 ± 0.08	76.8 ± 0.09	70.64 ± 0.07	71.2 ± 0.09	69.16 ± 0.08
		Cityblock	79.7 ± 0.09	75.83 ± 0.07	79.02 ± 0.08	76.23 ± 0.07	77.02 ± 0.07	75.83 ± 0.07
	MLM	Euclidean	79.53 ± 0.13	72.5 ± 0.1	78.47 ± 0.11	73.44 ± 0.1	74.68 ± 0.1	72.5 ± 0.1
		Mahalanobis	77.69 ± 0.11	71.66 ± 0.08	77.22 ± 0.09	72.47 ± 0.07	73.57 ± 0.08	71.66 ± 0.08
	MLM-NN	Cityblock	79.7 ± 0.09	75.83 ± 0.07	79.02 ± 0.08	76.23 ± 0.07	77.02 ± 0.07	75.83 ± 0.07
		Euclidean	79.53 ± 0.13	72.5 ± 0.1	78.47 ± 0.11	73.44 ± 0.1	74.68 ± 0.1	72.5 ± 0.1
	MLP	Mahalanobis	77.69 ± 0.11	71.66 ± 0.08	77.22 ± 0.09	72.47 ± 0.07	73.57 ± 0.08	71.66 ± 0.08
		Linear	66.97 ± 0.29	64.16 ± 0.11	79.02 ± 0.13	67.77 ± 0.09	61.61 ± 0.24	64.16 ± 0.11
Laplace	SVM	Linear	78.09 ± 0.11	71.66 ± 0.08	77.77 ± 0.08	72.7 ± 0.07	73.71 ± 0.08	71.66 ± 0.08
		RBF	80.35 ± 0.11	69.16 ± 0.06	79.58 ± 0.08	71.21 ± 0.05	72.74 ± 0.06	69.16 ± 0.06
	Bayes	Bayes	90.5 ± 0.08	79.16 ± 0.11	88.19 ± 0.07	80.78 ± 0.09	82.63 ± 0.09	79.16 ± 0.11
		Linear	93.11 ± 0.06	87.5 ± 0.1	91.52 ± 0.07	87.95 ± 0.1	89.15 ± 0.09	87.5 ± 0.1
	LSSVM	RBF	83.9 ± 0.1	80 ± 0.08	82.77 ± 0.09	80.26 ± 0.08	81.13 ± 0.09	80 ± 0.08
		Cityblock	86.07 ± 0.03	84.71 ± 0.03	85.68 ± 0.03	84.79 ± 0.03	85.11 ± 0.03	85.11 ± 0.03
		MLM	75.7 ± 0.05	75.14 ± 0.05	75.7 ± 0.05	75.21 ± 0.05	75.32 ± 0.05	75.32 ± 0.05
	MLM-NN	Euclidean	83.26 ± 0.03	81.85 ± 0.03	82.93 ± 0.03	81.95 ± 0.03	82.28 ± 0.03	82.28 ± 0.03
		Mahalanobis	83.26 ± 0.03	81.85 ± 0.03	82.93 ± 0.03	81.95 ± 0.03	82.28 ± 0.03	82.28 ± 0.03
	MLP	Cityblock	86.07 ± 0.03	84.71 ± 0.03	85.68 ± 0.03	84.79 ± 0.03	85.11 ± 0.03	85.11 ± 0.03
		Linear	77.92 ± 0.27	71.66 ± 0.12	83.33 ± 0.06	74.36 ± 0.08	70.6 ± 0.25	71.66 ± 0.12
Sobel	SVM	RBF	92.23 ± 0.02	77.5 ± 0.07	88.75 ± 0.01	79.14 ± 0.06	81.94 ± 0.05	77.5 ± 0.07
		Bayes	93.53 ± 0.01	68.33 ± 0.08	89.72 ± 0.02	72.75 ± 0.05	76.24 ± 0.05	68.33 ± 0.08
	LSSVM	Linear	93.11 ± 0.07	90.83 ± 0.09	92.36 ± 0.08	90.95 ± 0.09	91.48 ± 0.08	90.83 ± 0.09
		RBF	97.61 ± 0.03	96.66 ± 0.04	97.22 ± 0.03	96.68 ± 0.04	96.92 ± 0.03	96.66 ± 0.04
	MLM	Cityblock	95.38 ± 0.07	93.33 ± 0.09	94.72 ± 0.07	93.45 ± 0.09	93.92 ± 0.08	93.33 ± 0.09
		Euclidean	97.73 ± 0.03	95.83 ± 0.07	97.08 ± 0.04	95.93 ± 0.06	96.37 ± 0.06	95.83 ± 0.07
		Mahalanobis	93.5 ± 0.09	92.5 ± 0.09	93.19 ± 0.09	92.55 ± 0.09	92.78 ± 0.09	92.5 ± 0.09
	MLM-NN	Cityblock	97.73 ± 0.03	95.83 ± 0.07	97.08 ± 0.04	95.93 ± 0.06	96.37 ± 0.06	95.83 ± 0.07
		Euclidean	90.61 ± 0.11	89.16 ± 0.11	90.13 ± 0.11	89.24 ± 0.11	89.58 ± 0.11	89.16 ± 0.11
	MLP	Mahalanobis	93.5 ± 0.09	92.5 ± 0.09	93.19 ± 0.09	92.55 ± 0.09	92.78 ± 0.09	92.5 ± 0.09
		Linear	92.66 ± 0.09	90.83 ± 0.09	92.08 ± 0.09	90.93 ± 0.09	91.35 ± 0.09	90.83 ± 0.09
	SVM	RBF	98.33 ± 0.03	96.66 ± 0.07	97.77 ± 0.04	96.76 ± 0.06	97.14 ± 0.06	96.66 ± 0.07

used the evaluation metrics based on the classification results of the confusion matrix. The confusion matrix results include True Positive (TP), True Negative (TN), False Positive (FP) and False Negative (FN) some of which were used for the evaluation metrics.

Specificity (Spe) is the metric that measures the proportion of the results classified as negative among all the results that are really negative and is presented by Eq. (23). In the case of the skin lesion

classification, this metric corresponds to the correct percentage of the patient which really not have cancer.

$$\text{Spe} = \frac{\text{TN}}{\text{TN} + \text{FP}} \quad (23)$$

The sensitivity (Sen) represents the proportion of the results classified as positive among all the results that are actually positive and

**Table 3**

Result of classification of dermoscopy images from the ISIC 2016 dataset using LBP, GLCM, and HU considering the specificity (Spe), sensibility (Sen), positive predictive value (Ppv), F score, harmonic mean (Hm) and accuracy (Acc) as evaluation metrics.

Feature	Classifier	Setup	Spe(%)	Sen(%)	Ppv(%)	F score(%)	Hm(%)	Acc(%)
LBP	SVM	Linear	92.93 ± 0.01	89.57 ± 0.04	91.73 ± 0.02	89.73 ± 0.04	90.51 ± 0.03	90.51 ± 0.03
		RBF	89.04 ± 0.03	72.85 ± 0.02	85.95 ± 0.02	74.8 ± 0.02	77.85 ± 0.02	72.85 ± 0.02
	MLP		93.77 ± 0.02	92.42 ± 0.03	93.24 ± 0.02	92.46 ± 0.03	92.79 ± 0.02	92.42 ± 0.03
		Mahalanobis	88.75 ± 0.04	88 ± 0.04	88.49 ± 0.04	88.03 ± 0.04	88.21 ± 0.04	88 ± 0.04
	MLM-NN	Euclidean	89.14 ± 0.02	88.42 ± 0.02	88.91 ± 0.02	88.46 ± 0.02	88.63 ± 0.02	88.42 ± 0.02
		Cityblock	91.49 ± 0.03	90.28 ± 0.03	91.02 ± 0.02	90.32 ± 0.03	90.61 ± 0.03	90.28 ± 0.03
	MLM	Mahalanobis	88.75 ± 0.04	88 ± 0.04	88.49 ± 0.04	88.03 ± 0.04	88.21 ± 0.04	88 ± 0.04
		Euclidean	89.14 ± 0.02	88.42 ± 0.02	88.91 ± 0.02	88.46 ± 0.02	88.63 ± 0.02	88.42 ± 0.02
	LSSVM	Cityblock	91.49 ± 0.03	90.28 ± 0.03	91.02 ± 0.02	90.32 ± 0.03	90.61 ± 0.03	90.28 ± 0.03
		Linear	88.78 ± 0.02	85.57 ± 0.03	87.79 ± 0.02	85.75 ± 0.03	86.5 ± 0.03	85.57 ± 0.03
HU	RBF	RBF	89.06 ± 0.03	72.71 ± 0.02	85.96 ± 0.02	74.69 ± 0.02	77.76 ± 0.02	72.71 ± 0.02
		Bayes	85.56 ± 0.02	84.57 ± 0.03	85.32 ± 0.03	84.64 ± 0.03	84.86 ± 0.03	84.57 ± 0.03
	SVM	Linear	94.24 ± 0.02	93.71 ± 0.02	94.01 ± 0.02	93.72 ± 0.02	93.85 ± 0.02	93.71 ± 0.02
		RBF	97.08 ± 0	56.28 ± 0.01	94.56 ± 0.01	66.69 ± 0	69.59 ± 0	56.28 ± 0.01
	MLP		92.71 ± 0.01	90.14 ± 0.03	91.77 ± 0.02	90.25 ± 0.03	90.86 ± 0.03	90.14 ± 0.03
		Mahalanobis	92.48 ± 0.02	92 ± 0.01	92.27 ± 0.01	92 ± 0.01	92.12 ± 0.01	92 ± 0.01
	MLM-NN	Euclidean	92.48 ± 0.02	92 ± 0.01	92.27 ± 0.01	92 ± 0.01	92.12 ± 0.01	92 ± 0.01
		Cityblock	91.01 ± 0.02	90.28 ± 0.02	90.75 ± 0.02	90.31 ± 0.02	90.49 ± 0.02	90.28 ± 0.02
	MLM	Mahalanobis	92.48 ± 0.02	92 ± 0.01	92.27 ± 0.01	92 ± 0.01	92.12 ± 0.01	92 ± 0.01
		Euclidean	92.48 ± 0.02	92 ± 0.01	92.27 ± 0.01	92 ± 0.01	92.12 ± 0.01	92 ± 0.01
	LSSVM	Cityblock	91.01 ± 0.02	90.28 ± 0.02	90.75 ± 0.02	90.31 ± 0.02	90.49 ± 0.02	90.28 ± 0.02
		Linear	90.24 ± 0.02	80.85 ± 0.03	87.56 ± 0.01	81.56 ± 0.03	83.61 ± 0.02	80.85 ± 0.03
GLCM	Bayes	RBF	91.29 ± 0.01	79.71 ± 0.04	88.04 ± 0.01	80.66 ± 0.03	83.12 ± 0.03	79.71 ± 0.04
		Bayes	92.04 ± 0	72.85 ± 0.02	87.74 ± 0	75.09 ± 0.02	78.68 ± 0.01	72.85 ± 0.02
	SVM	Linear	93.36 ± 0.03	90.85 ± 0.04	92.41 ± 0.03	90.94 ± 0.04	91.55 ± 0.03	90.85 ± 0.04
		RBF	85.03 ± 0.04	79.85 ± 0.04	83.93 ± 0.03	80.32 ± 0.04	81.43 ± 0.04	79.85 ± 0.04
	MLP		93.62 ± 0.03	92.42 ± 0.04	93.14 ± 0.03	92.46 ± 0.04	92.75 ± 0.04	92.42 ± 0.04
		Mahalanobis	89.08 ± 0.04	88.28 ± 0.03	88.8 ± 0.03	88.31 ± 0.03	88.51 ± 0.03	88.28 ± 0.03
	MLM-NN	Euclidean	85.94 ± 0.03	85.28 ± 0.03	85.74 ± 0.03	85.32 ± 0.03	85.47 ± 0.03	85.28 ± 0.03
		Cityblock	87.43 ± 0.04	87 ± 0.04	87.27 ± 0.04	87.01 ± 0.04	87.12 ± 0.04	87 ± 0.04
	MLM	Mahalanobis	89.08 ± 0.04	88.28 ± 0.03	88.8 ± 0.03	88.31 ± 0.03	88.51 ± 0.03	88.28 ± 0.03
		Euclidean	85.94 ± 0.03	85.28 ± 0.03	85.74 ± 0.03	85.32 ± 0.03	85.47 ± 0.03	85.28 ± 0.03
	LSSVM	Cityblock	87.43 ± 0.04	87 ± 0.04	87.27 ± 0.04	87.01 ± 0.04	87.12 ± 0.04	87 ± 0.04
		Linear	92.63 ± 0.03	89.71 ± 0.04	91.56 ± 0.03	89.83 ± 0.04	90.52 ± 0.04	89.71 ± 0.04
	Bayes	RBF	84.84 ± 0.04	78.14 ± 0.04	83.54 ± 0.03	78.79 ± 0.03	80.2 ± 0.03	78.14 ± 0.04
		Bayes	90.05 ± 0.03	83.57 ± 0.05	88.13 ± 0.03	84.02 ± 0.04	85.46 ± 0.04	83.57 ± 0.05

presented by Eq. (24). In diagnostic problems, this is one of the most important metrics, indicating if the patient has the disease. One can see that if the classification is not correct, the patient is no longer treated because he is informed that he has no disease.

$$\text{Sen} = \frac{\text{TP}}{\text{TP} + \text{FN}} \quad (24)$$

The positive predictive value (Ppv) is the probability of true positives in relation to all the results classified as positive and is presented by Eq. (25). Even if the diagnostic of the test was positive, this metric calculates a probability of the test be coherent with the prior probability.

$$\text{Ppv} = \frac{\text{TP}}{\text{TP} + \text{FP}} \quad (25)$$

As a counterpoint to Ppv, considering its risk of imbalance, the *F* score calculates the weighted mean harmonic value between Ppv and Sen and is presented by Eq. (26). This represents the performance of the method since although a diagnosis is classified accurately, it does not

indicate that it will have the same performance for the other data.

$$F \text{ Score} = \frac{2 \times \text{Sen} \times \text{Ppv}}{\text{Sen} + \text{Ppv}} \quad (26)$$

In this work the harmonic mean (Hm) of the specificity and the sensitivity was also calculated and is presented by Eq. (27). This metric represents whether the whole rating is balanced.

$$\text{Hm} = \frac{2 \times \text{Sen} \times \text{Esp}}{\text{Sen} + \text{Esp}} \quad (27)$$

The Accuracy (Acc) reveals the proximity of the result to the gold standard by the relationship between the hits and the set of possibilities of errors and correctness and is presented by Eq. (28).

$$\text{Acc} = \frac{\text{TP} + \text{TN}}{\text{TP} + \text{TN} + \text{FP} + \text{FN}} \quad (28)$$

**Table 4**

Result of classification of dermoscopy images from the ISIC 2016 dataset using SCM considering the specificity (Spe), sensibility (Sen), positive predictive value (Ppv), F score, harmonic mean (Hm) and accuracy (Acc) as evaluation metrics.

Filter	Classifier	Setup	Spe(%)	Sen(%)	Ppv(%)	F score(%)	Hm(%)	Acc(%)
Fourier	LSSVM	Bayes	92.71 ± 0.02	91.28 ± 0.04	92.22 ± 0.03	91.35 ± 0.04	91.69 ± 0.03	91.28 ± 0.04
		Linear	94.62 ± 0.02	93.85 ± 0.02	94.29 ± 0.02	93.87 ± 0.02	94.06 ± 0.02	93.85 ± 0.02
		RBF	89.81 ± 0.02	88.71 ± 0.03	89.46 ± 0.02	88.77 ± 0.03	89.03 ± 0.03	88.71 ± 0.03
	MLM	Cityblock	85.79 ± 0.04	84.85 ± 0.04	85.53 ± 0.04	84.91 ± 0.04	85.13 ± 0.04	84.85 ± 0.04
		Euclidean	86.08 ± 0.04	85.28 ± 0.04	85.86 ± 0.04	85.33 ± 0.04	85.52 ± 0.04	85.28 ± 0.04
		Mahalanobis	85.86 ± 0.03	85 ± 0.04	85.63 ± 0.03	85.05 ± 0.04	85.25 ± 0.03	85 ± 0.04
	MLM-NN	Cityblock	85.79 ± 0.04	84.85 ± 0.04	85.53 ± 0.04	84.91 ± 0.04	85.13 ± 0.04	84.85 ± 0.04
		Euclidean	86.08 ± 0.04	85.28 ± 0.04	85.86 ± 0.04	85.33 ± 0.04	85.52 ± 0.04	85.28 ± 0.04
		Mahalanobis	85.86 ± 0.03	85 ± 0.04	85.63 ± 0.03	85.05 ± 0.04	85.25 ± 0.03	85 ± 0.04
	MLP	Linear	92.65 ± 0.02	90.42 ± 0.04	91.85 ± 0.03	90.52 ± 0.04	91.05 ± 0.03	90.42 ± 0.04
		RBF	92.99 ± 0.02	91.14 ± 0.04	92.32 ± 0.03	91.21 ± 0.04	91.66 ± 0.03	91.14 ± 0.04
Gaussian	LSSVM	Bayes	79.81 ± 0.03	77.28 ± 0.02	79.45 ± 0.03	77.53 ± 0.02	78.08 ± 0.02	77.28 ± 0.02
		Linear	80.92 ± 0.04	76.71 ± 0.04	80.37 ± 0.04	77.16 ± 0.04	78.04 ± 0.04	76.71 ± 0.04
		RBF	78.43 ± 0.03	77 ± 0.04	78.44 ± 0.03	77.19 ± 0.04	77.47 ± 0.04	77 ± 0.04
	MLM	Cityblock	82.48 ± 0.04	81.85 ± 0.04	82.35 ± 0.04	81.9 ± 0.04	82.04 ± 0.04	81.85 ± 0.04
		Euclidean	79.29 ± 0.03	78.42 ± 0.03	79.17 ± 0.03	78.51 ± 0.03	78.7 ± 0.03	78.42 ± 0.03
		Mahalanobis	82.53 ± 0.02	82 ± 0.02	82.41 ± 0.02	82.03 ± 0.02	82.16 ± 0.02	82 ± 0.02
	MLM-NN	Cityblock	82.48 ± 0.04	81.85 ± 0.04	82.35 ± 0.04	81.9 ± 0.04	82.04 ± 0.04	81.85 ± 0.04
		Euclidean	79.29 ± 0.03	78.42 ± 0.03	79.17 ± 0.03	78.51 ± 0.03	78.7 ± 0.03	78.42 ± 0.03
		Mahalanobis	82.53 ± 0.02	82 ± 0.02	82.41 ± 0.02	82.03 ± 0.02	82.16 ± 0.02	82 ± 0.02
	MLP	Linear	87.01 ± 0.03	5.14 ± 0.02	86.41 ± 0.02	85.25 ± 0.02	85.68 ± 0.02	85.14 ± 0.02
		RBF	85.28 ± 0.02	84.42 ± 0.02	85.05 ± 0.02	84.48 ± 0.02	84.68 ± 0.02	84.42 ± 0.02
Laplace	LSSVM	Bayes	75.59 ± 0.07	72.71 ± 0.09	76.88 ± 0.05	73.48 ± 0.08	73.75 ± 0.08	72.71 ± 0.09
		Linear	79.4 ± 0.03	78.57 ± 0.04	79.35 ± 0.03	78.66 ± 0.03	78.84 ± 0.03	78.57 ± 0.04
		RBF	79.2 ± 0.03	76.57 ± 0.04	79.12 ± 0.03	76.93 ± 0.04	77.43 ± 0.04	76.57 ± 0.04
	MLM	Cityblock	86.07 ± 0.03	84.71 ± 0.03	85.68 ± 0.03	84.79 ± 0.03	85.11 ± 0.03	84.71 ± 0.03
		Euclidean	75.7 ± 0.05	75.14 ± 0.05	75.7 ± 0.05	75.21 ± 0.05	75.32 ± 0.05	75.14 ± 0.05
		Mahalanobis	83.26 ± 0.03	81.85 ± 0.03	82.93 ± 0.03	81.95 ± 0.03	82.28 ± 0.03	81.85 ± 0.03
	MLM-NN	Cityblock	86.07 ± 0.03	84.71 ± 0.03	85.68 ± 0.03	84.79 ± 0.03	85.11 ± 0.03	84.71 ± 0.03
		Euclidean	75.7 ± 0.05	75.14 ± 0.05	75.7 ± 0.05	75.21 ± 0.05	75.32 ± 0.05	75.14 ± 0.05
		Mahalanobis	83.26 ± 0.03	81.85 ± 0.03	82.93 ± 0.03	81.95 ± 0.03	82.28 ± 0.03	81.85 ± 0.03
	MLP	Linear	84.84 ± 0.05	83.57 ± 0.04	84.49 ± 0.04	83.64 ± 0.04	83.94 ± 0.04	83.57 ± 0.04
		RBF	84.9 ± 0.04	83.57 ± 0.04	84.52 ± 0.04	83.64 ± 0.04	83.96 ± 0.04	83.57 ± 0.04
	SVM	Linear	84.17 ± 0.07	65.14 ± 0.04	84.71 ± 0.03	69.07 ± 0.02	71.47 ± 0.04	65.14 ± 0.04
		RBF	79.38 ± 0.03	76.85 ± 0.04	79.27 ± 0.03	77.19 ± 0.04	77.68 ± 0.03	76.85 ± 0.04
Sobel	LSSVM	Bayes	74.07 ± 0.05	72.71 ± 0.05	74.29 ± 0.05	72.95 ± 0.05	73.18 ± 0.05	72.71 ± 0.05
		Linear	85.56 ± 0.02	84.57 ± 0.03	85.28 ± 0.02	84.63 ± 0.03	84.86 ± 0.02	84.57 ± 0.03
		RBF	78.8 ± 0.05	71.71 ± 0.03	78.49 ± 0.04	72.72 ± 0.02	74.03 ± 0.03	71.71 ± 0.03
	MLM	Cityblock	80.36 ± 0.05	79.57 ± 0.05	80.18 ± 0.05	79.63 ± 0.05	79.81 ± 0.05	79.57 ± 0.05
		Euclidean	77.42 ± 0.04	76.85 ± 0.04	77.37 ± 0.04	76.91 ± 0.04	77.03 ± 0.04	76.85 ± 0.04
		Mahalanobis	80.33 ± 0.04	79.28 ± 0.03	80.16 ± 0.03	79.37 ± 0.03	79.61 ± 0.03	79.28 ± 0.03
	MLM-NN	Cityblock	80.36 ± 0.05	79.57 ± 0.05	80.18 ± 0.05	79.63 ± 0.05	79.81 ± 0.05	79.57 ± 0.05
		Euclidean	77.42 ± 0.04	76.85 ± 0.04	77.37 ± 0.04	76.91 ± 0.04	77.03 ± 0.04	76.85 ± 0.04
		Mahalanobis	80.33 ± 0.04	79.28 ± 0.03	80.16 ± 0.03	79.37 ± 0.03	79.61 ± 0.03	79.28 ± 0.03
	MLP	Linear	82.03 ± 0.04	81.57 ± 0.04	81.91 ± 0.04	81.6 ± 0.04	81.7 ± 0.04	81.57 ± 0.04
		RBF	85.11 ± 0.02	83.57 ± 0.03	84.71 ± 0.02	83.67 ± 0.02	84.03 ± 0.02	83.57 ± 0.03
	SVM	Linear	77.65 ± 0.04	71.57 ± 0.03	77.77 ± 0.03	72.54 ± 0.03	73.6 ± 0.03	71.57 ± 0.03

### 3. Results and discussion

Considering the Spe, Sen, Ppv, F Score, Hm and Acc metrics and the dermoscopy images, this section is divided into 2 steps, the first step is the evaluation of the SCM compared to the extraction methods described in Section 2.4 and the second step the evaluation of the SCM with recent related works. The entire process related to SCM is presented in Fig. 8.

The hyperparameters for the MLP, SVM, and LSSVM were selected from cross-validation with 10-folds. Both SVM and LSSVM were trained by the Matlab 2015a SVM toolbox. For each hyper-parameter, a greedy

log search was used between  $2^2$  and  $2^{11}$ . For these configurations, both Linear kernel and Radial Basis Function kernel were used. MLP was trained using the Levenberg-Marquardt optimization and the Hidden layer varied from 1 to 50. For all datasets, the SCM was tested with the Gaussian, Laplacian, and Sobel filters with different kernel sizes ( $3 \times 3$  up to  $15 \times 15$ ). The Gaussian filter was varied from 0.5 to 5 as its standard deviation. This work presents only the best results of each configuration.

The process for each of the filters used in this work is illustrated in Fig. 9. Each of the filters used modifies the structure of the image where the SCM later highlights the most relevant features in each combination

**Table 5**

Result of classification of dermoscopy images from the ISIC 2017 dataset using LBP, GLCM, and HU considering the specificity (Spe), sensibility (Sen), positive predictive value (Ppv), F score, harmonic mean (Hm) and accuracy (Acc) as evaluation metrics.

Feature	Classifier	Setup	Spe(%)	Sen(%)	Ppv(%)	F score(%)	Hm(%)	Acc(%)
LBP	SVM	Linear	89.32 ± 0	78.24 ± 0.03	86.62 ± 0	79.26 ± 0.03	81.57 ± 0.02	78.24 ± 0.03
		RBF	78.94 ± 0.02	72.6 ± 0.04	79.01 ± 0.01	73.56 ± 0.03	74.71 ± 0.03	72.6 ± 0.04
	MLP		90.16 ± 0.01	88 ± 0.01	89.37 ± 0.01	88.08 ± 0.01	88.06 ± 0.01	88 ± 0.01
		Mahalanobis	86.4 ± 0.01	84.6 ± 0.01	85.86 ± 0.01	84.69 ± 0.01	85.12 ± 0	84.6 ± 0.01
	MLM-NN	Euclidean	84.44 ± 0.02	83.93 ± 0.01	84.29 ± 0.01	83.96 ± 0.01	84.08 ± 0.01	83.93 ± 0.01
		Cityblock	84.68 ± 0.02	84.53 ± 0.01	84.64 ± 0.01	84.54 ± 0.01	84.57 ± 0.01	84.53 ± 0.01
	MLM	Mahalanobis	86.4 ± 0.01	84.6 ± 0.01	85.86 ± 0.01	84.69 ± 0.01	85.12 ± 0	84.6 ± 0.01
		Euclidean	84.44 ± 0.02	83.93 ± 0.01	84.29 ± 0.01	83.96 ± 0.01	84.08 ± 0.01	83.93 ± 0.01
	LSSVM	Cityblock	84.68 ± 0.02	84.53 ± 0.01	84.64 ± 0.01	84.54 ± 0.01	84.57 ± 0.01	84.53 ± 0.01
		Linear	86.09 ± 0.02	79.66 ± 0.02	84.59 ± 0.01	80.21 ± 0.02	81.61 ± 0.02	79.66 ± 0.02
HU	SVM	RBF	79.22 ± 0.02	72.46 ± 0.03	79.24 ± 0.01	73.48 ± 0.03	74.71 ± 0.03	72.46 ± 0.03
		Bayes	85.18 ± 0.02	84.2 ± 0.02	84.9 ± 0.02	84.25 ± 0.02	84.49 ± 0.02	84.2 ± 0.02
	MLP	Linear	91.08 ± 0.01	86 ± 0.02	89.33 ± 0.01	86.25 ± 0.02	87.44 ± 0.02	86 ± 0.02
		RBF	89.22 ± 0.31	51.6 ± 0.01	98.47 ± 0.01	66.45 ± 0	60.72 ± 0.21	51.6 ± 0.01
	MLM	Mahalanobis	91.69 ± 0.01	87.4 ± 0.02	90.14 ± 0.01	87.58 ± 0.02	88.06 ± 0.01	87.4 ± 0.02
		Euclidean	80.34 ± 0.02	80.2 ± 0.03	80.32 ± 0.02	80.21 ± 0.03	80.24 ± 0.03	80.2 ± 0.03
	MLM-NN	Cityblock	80.1 ± 0.03	79.93 ± 0.03	80.07 ± 0.03	79.94 ± 0.03	79.98 ± 0.03	79.93 ± 0.03
		Mahalanobis	80.34 ± 0.02	80.2 ± 0.03	80.32 ± 0.02	80.21 ± 0.03	80.24 ± 0.03	80.2 ± 0.03
	LSSVM	Euclidean	80.34 ± 0.02	80.2 ± 0.03	80.32 ± 0.02	80.21 ± 0.03	80.24 ± 0.03	80.2 ± 0.03
		Cityblock	80.1 ± 0.03	79.93 ± 0.03	80.07 ± 0.03	79.94 ± 0.03	79.98 ± 0.03	79.93 ± 0.03
	Bayes	Linear	91.75 ± 0	75.06 ± 0.02	87.65 ± 0	76.79 ± 0.02	80.08 ± 0.01	75.06 ± 0.02
		RBF	90.69 ± 0.01	72.73 ± 0.03	87.02 ± 0	74.88 ± 0.02	78.24 ± 0.02	72.73 ± 0.03
GLCM	SVM	Bayes	94.32 ± 0	63.53 ± 0.02	90.21 ± 0.01	69.2 ± 0.01	73.29 ± 0.01	63.53 ± 0.02
		Linear	89.19 ± 0.01	85.94 ± 0.01	88.11 ± 0.01	86.1 ± 0.01	86.87 ± 0.01	85.94 ± 0.01
	MLP	RBF	78.93 ± 0.41	52.22 ± 0.02	97.96 ± 0.01	66.49 ± 0	54.35 ± 0.28	52.22 ± 0.02
		Mahalanobis	77.76 ± 0.27	80.74 ± 0.11	87.1 ± 0.06	82.51 ± 0.06	76.32 ± 0.27	80.74 ± 0.11
	MLM-NN	Euclidean	86.33 ± 0.02	85.33 ± 0.02	86.02 ± 0.02	85.38 ± 0.02	85.62 ± 0.02	85.33 ± 0.02
		Cityblock	80.9 ± 0.02	80.27 ± 0.02	80.77 ± 0.02	80.32 ± 0.02	80.46 ± 0.02	80.27 ± 0.02
	MLM	Mahalanobis	86.33 ± 0.02	85.33 ± 0.02	86.02 ± 0.02	85.38 ± 0.02	85.62 ± 0.02	85.33 ± 0.02
		Euclidean	85.06 ± 0.02	84.32 ± 0.02	84.85 ± 0.02	84.36 ± 0.02	84.54 ± 0.02	84.32 ± 0.02
	LSSVM	Cityblock	80.9 ± 0.02	80.27 ± 0.02	80.77 ± 0.02	80.32 ± 0.02	80.46 ± 0.02	80.27 ± 0.02
		Linear	88.79 ± 0.01	84.86 ± 0.01	87.53 ± 0	85.07 ± 0.01	85.99 ± 0	84.86 ± 0.01
	Bayes	RBF	82.25 ± 0.02	81.62 ± 0.02	82.14 ± 0.02	81.67 ± 0.02	81.81 ± 0.02	81.62 ± 0.02
		Bayes	86.74 ± 0.02	72.56 ± 0.03	84.64 ± 0.01	74.38 ± 0.02	77.02 ± 0.02	72.56 ± 0.03

of original image and filtered image.

**Table 1** shows the results of the classification using the PH2 dataset. The attributes extracted from the LBP were superior to the other methods, where the maximum values of the characteristics were from the MLM classifier using the Cityblock and Euclidean distances in all the evaluation metrics.

The accuracy result of 98.33% may indicate that the plurilateral assessed texture has a higher degree of discrimination than with GLCM, but also reinforces the technique used by the specialists since the normalization of the tone of skin has helped the LBP reach a result closer to the ABCD method. Regarding specificity and sensitivity, the LBP also had a balanced outcome, not favoring the malignant or benign class of the lesion with 98.8% and 98.33% respectively, which also reinforces its ability to discriminate the data. The result of the GLCM application in the PH2 dataset illustrates that despite the efficiency of the method, it has lower overall results than LBP. By hypothesis, analyzing the behavior of the extractor, this data indicates that at some point it may be losing information due to its unilateral relationship between pixels for the creation of the co-occurrence matrix.

Except for the Linear SVM and Linear LSSVM, Moments of HU did not show significant results for LBP and GLCM. Observing the Specificity, the results of the classifiers show a greater tendency to

classify the lesion as non-melanoma.

The SCM showed the best results for the lesion classification results presented in **Table 1**. **Table 2** illustrates results of the melanoma metrics of the SCM applied to the PH2 dataset.

The highest values of the SCM with the function  $k$  in the frequency domain using Linear SVM and RBF respectively had a specificity and sensitivity of 99.4% and 99.16%, in addition to PPV and F-score of 99, 3% and 99.17% indicating a consistent results. This technique also showed a high accuracy of 99.16% indicating the efficiency of this extractor. Interestingly, since the magnitude spectrum has frequencies closer to the DC component and therefore low frequencies, the Laplace and Sobel high-frequency filters also showed high hit rates. This result shows that melanoma can be identified by both the lesion region and its border (high frequencies) or color variation (medium and low frequencies). This idea is reinforced when the results of the Gaussian filter show slightly lower values in the MLM and MLM-NN classifiers when compared to the Laplacian filter. As the ABCD technique analyzes these lesion characteristics accurately, the SCM analysis based on the most relevant components in the frequency domain gives results very close to those of the specialist(s).

The HU Moments using the ISIC 2016 dataset, obtained the best accuracy result with a 93.71% hit rate and 94.01% and 93.72% for Ppv

**Table 6**

Result of classification of dermoscopy images from the ISIC 2017 dataset using SCM considering the specificity (Spe), sensibility (Sen), positive predictive value (Ppv), F score, harmonic mean (Hm) and accuracy (Acc) as evaluation metrics.

Filter	Classifier	Setup	Spe(%)	Sen(%)	Ppv(%)	F score(%)	Hm(%)	Acc(%)
Fourier	LSSVM	Bayes	88.84 ± 0.01	80.06 ± 0.03	86.59 ± 0.01	80.78 ± 0.03	82.68 ± 0.03	80.06 ± 0.03
		Linear	92.15 ± 0.01	89.93 ± 0.01	91.29 ± 0.01	90 ± 0.01	90.54 ± 0.01	89.93 ± 0.01
		RBF	87.37 ± 0.02	83.17 ± 0.03	86.21 ± 0.02	83.44 ± 0.03	84.41 ± 0.02	83.17 ± 0.03
		Cityblock	77.05 ± 0.03	76.68 ± 0.03	77.03 ± 0.03	76.73 ± 0.03	76.8 ± 0.03	76.68 ± 0.03
	MLM	Euclidean	80.6 ± 0.03	80.33 ± 0.03	80.57 ± 0.03	80.36 ± 0.03	80.42 ± 0.03	80.33 ± 0.03
		Mahalanobis	78.93 ± 0.03	78.58 ± 0.03	78.88 ± 0.03	78.61 ± 0.03	78.69 ± 0.03	78.58 ± 0.03
	MLM-NN	Euclidean	80.6 ± 0.03	80.33 ± 0.03	80.57 ± 0.03	80.36 ± 0.03	80.42 ± 0.03	80.33 ± 0.03
		Mahalanobis	78.93 ± 0.03	78.58 ± 0.03	78.88 ± 0.03	78.61 ± 0.03	78.69 ± 0.03	78.58 ± 0.03
	MLP	Euclidean	80.34 ± 0.28	79.05 ± 0.1	88.5 ± 0.04	81.14 ± 0.05	75.89 ± 0.26	79.05 ± 0.1
		Linear	89.74 ± 0.01	79.79 ± 0.04	87.14 ± 0.01	80.62 ± 0.03	82.75 ± 0.03	79.79 ± 0.04
Gaussian	SVM	RBF	91.72 ± 0.01	71.14 ± 0.03	87.63 ± 0	73.79 ± 0.02	77.48 ± 0.02	71.14 ± 0.03
		Bayes	92.8 ± 0.03	62.97 ± 0.03	89.66 ± 0.03	68.7 ± 0.02	72.53 ± 0.03	62.97 ± 0.03
		Linear	86.74 ± 0.03	75.67 ± 0.03	84.68 ± 0.02	76.9 ± 0.03	79.09 ± 0.03	75.67 ± 0.03
		RBF	82.96 ± 0.05	80.4 ± 0.04	82.41 ± 0.04	80.61 ± 0.04	81.18 ± 0.04	80.4 ± 0.04
	MLM	Cityblock	75.99 ± 0.03	75.2 ± 0.03	75.97 ± 0.03	75.29 ± 0.03	75.46 ± 0.03	75.2 ± 0.03
		Euclidean	75.18 ± 0.03	74.79 ± 0.03	75.21 ± 0.03	74.85 ± 0.03	74.92 ± 0.03	74.79 ± 0.03
	MLM-NN	Mahalanobis	74.22 ± 0.02	73.91 ± 0.02	74.21 ± 0.02	73.95 ± 0.02	74.01 ± 0.02	73.91 ± 0.02
		Cityblock	75.99 ± 0.03	75.2 ± 0.03	75.97 ± 0.03	75.29 ± 0.03	75.46 ± 0.03	75.2 ± 0.03
	MLP	Euclidean	75.18 ± 0.03	74.79 ± 0.03	75.21 ± 0.03	74.85 ± 0.03	74.92 ± 0.03	74.79 ± 0.03
		Mahalanobis	74.22 ± 0.02	73.91 ± 0.02	74.21 ± 0.02	73.95 ± 0.02	74.01 ± 0.02	73.91 ± 0.02
	SVM	Linear	84.58 ± 0.03	76.08 ± 0.03	83.27 ± 0.02	77.02 ± 0.03	78.74 ± 0.03	76.08 ± 0.03
		RBF	80 ± 0	73.04 ± 0.02	79.72 ± 0.01	74 ± 0	75.31 ± 0.01	73.04 ± 0.02
Laplace	LSSVM	Bayes	74.38 ± 0.03	64.53 ± 0.03	77.4 ± 0.02	67.03 ± 0.02	68.07 ± 0.02	64.53 ± 0.03
		Linear	76.16 ± 0.02	75.93 ± 0.02	76.17 ± 0.02	75.96 ± 0.02	76.01 ± 0.02	75.93 ± 0.02
		RBF	68.77 ± 0.04	67 ± 0.04	69.48 ± 0.04	67.41 ± 0.04	67.64 ± 0.04	67 ± 0.04
		Cityblock	73.61 ± 0.03	73.13 ± 0.03	73.64 ± 0.03	73.2 ± 0.03	73.29 ± 0.03	73.13 ± 0.03
	MLM	Euclidean	74.92 ± 0.03	74.46 ± 0.03	74.92 ± 0.03	74.52 ± 0.03	74.61 ± 0.03	74.46 ± 0.03
		Mahalanobis	75.02 ± 0.04	74.73 ± 0.04	75.02 ± 0.04	74.77 ± 0.04	74.83 ± 0.04	74.73 ± 0.04
	MLM-NN	Cityblock	73.61 ± 0.03	73.13 ± 0.03	73.64 ± 0.03	73.2 ± 0.03	73.29 ± 0.03	73.13 ± 0.03
		Euclidean	74.92 ± 0.03	74.46 ± 0.03	74.92 ± 0.03	74.52 ± 0.03	74.61 ± 0.03	74.46 ± 0.03
	MLP	Mahalanobis	75.02 ± 0.04	74.73 ± 0.04	75.02 ± 0.04	74.77 ± 0.04	74.83 ± 0.04	74.73 ± 0.04
		Linear	83.02 ± 0.03	80.26 ± 0.03	82.42 ± 0.03	80.48 ± 0.03	81.1 ± 0.03	80.26 ± 0.03
	SVM	RBF	78.53 ± 0.05	74.4 ± 0.09	80.12 ± 0.04	75.58 ± 0.07	75.89 ± 0.07	74.4 ± 0.09
		Linear	71.56 ± 0.02	69.2 ± 0.01	72.03 ± 0.02	69.65 ± 0.01	70.03 ± 0.01	69.2 ± 0.01
Sobel	LSSVM	Bayes	83.1 ± 0.02	80.33 ± 0.03	82.58 ± 0.02	80.57 ± 0.03	81.19 ± 0.02	80.33 ± 0.03
		Linear	84.84 ± 0.01	83.06 ± 0.02	84.39 ± 0.01	83.18 ± 0.02	83.59 ± 0.01	83.06 ± 0.02
		RBF	73.73 ± 0.03	71.46 ± 0.02	73.91 ± 0.02	71.81 ± 0.02	72.23 ± 0.02	71.46 ± 0.02
		Cityblock	76.4 ± 0.04	76.13 ± 0.04	76.39 ± 0.04	76.16 ± 0.04	76.22 ± 0.04	76.13 ± 0.04
	MLM	Euclidean	77.88 ± 0.03	77.4 ± 0.03	77.83 ± 0.03	77.45 ± 0.03	77.55 ± 0.03	77.4 ± 0.03
		Mahalanobis	80.16 ± 0.03	79.53 ± 0.03	80.07 ± 0.03	79.59 ± 0.03	79.73 ± 0.03	79.53 ± 0.03
	MLM-NN	Cityblock	76.4 ± 0.04	76.13 ± 0.04	76.39 ± 0.04	76.16 ± 0.04	76.22 ± 0.04	76.13 ± 0.04
		Euclidean	77.88 ± 0.03	77.4 ± 0.03	77.83 ± 0.03	77.45 ± 0.03	77.55 ± 0.03	77.4 ± 0.03
	MLP	Mahalanobis	80.16 ± 0.03	79.53 ± 0.03	80.07 ± 0.03	79.59 ± 0.03	79.73 ± 0.03	79.53 ± 0.03
		Linear	83.75 ± 0.03	81.53 ± 0.03	83.21 ± 0.03	81.69 ± 0.03	82.2 ± 0.03	81.53 ± 0.03
	SVM	RBF	88.3 ± 0.02	84.06 ± 0.02	86.99 ± 0.02	84.31 ± 0.02	85.29 ± 0.02	84.06 ± 0.02
		Linear	84.2 ± 0.01	80.13 ± 0.01	83.3 ± 0.01	80.46 ± 0.01	81.37 ± 0.01	80.13 ± 0.01

**Table 7**

Comparison of the SCM with recent methods using the same datasets and sensibility (Sen), specificity (Spe), accuracy (Acc) and area under the curve (AUC) as evaluation metrics.

Dataset	Method	Sen(%)	Spe(%)	Acc(%)	AUC(%)
PH2	Satheesha <i>et al.</i> [47]	96	97	95.75	-
	Bi <i>et al.</i> [48]	87.5	93.13	92	-
	Waheed <i>et al.</i> [16]	97	84	96	90
	Proposed Approach	99.4	99.2	99	99
ISIC 2016	Gutman <i>et al.</i> [27]	50	92	91.6	67
	Yu <i>et al.</i> [21]	-	-	83.09	79.57
	Yu <i>et al.</i> [20]	50	94	85	80.4
	Lopez <i>et al.</i> [49]	78.6	79.7	81.33	-
	Proposed Approach	95.23	94.57	94.5	92
ISIC 2017	Codella <i>et al.</i> [28]	71.8	90.1	-	92.6
	Matsunaga <i>et al.</i> [23]	-	-	-	95.8
	Sousa <i>et al.</i> [50]	63.3	90	84.7	84.6
	Li <i>et al.</i> [24]	50.4	93.3	85.2	82.3
	Proposed Approach	92.15	89.9	89.93	89

and *F*-score using the Linear SVM as shown in [Table 3](#). Also the Hu extractor was slightly better with the ISIC 2016 than with the PH2 database in all the metrics and its accuracy result was slightly superior to the other extractors. As justified in Section 2.1, some factors such as the location of the lesion as well as its size are not as good as those in the PH2 dataset and, given the invariance of the extractor HU, this result may be related to the discriminative capacity in relation to the area of the lesion, or that the ISIC 2016 dataset has more images where melanoma can also be identified at moments. The LBP and GLCM extractors with the MLP classifier obtained an accuracy very close to that of HU, with both reaching 92.42%. The LBP extractor with specificity of 93.77% and sensitivity of 92.42% underscores a balanced behavior between the discrimination for each class. This result is also significant due to the statistical behavior of GLCM with 93.62% and 92.42% specificity and sensitivity, respectively.

Applying different filters with SCM in the ISIC 2016 dataset, as illustrated in [Table 4](#), the SCM combined with the filter function *k* in the frequency domain presents the best result against the other filters with Spe 95.23%, Sen 94.57%, Ppv 94.94%, *F* score 94.58%, Hm 94.74% and Acc 94.57% using the classifier Linear SVM.

A similar behavior was observed in the other filters. The Gaussian, Laplace and Sobel filters reached a general statistic of 85% in all the metrics suggesting that the dermoscopy images that contain melanoma have a homogeneous behavior in their characteristics.

The domain change of the function *k* and the proposed method is more robust to the presence of noise, since it has a discriminative power that helps highlight the most important frequencies of the image.

For the ISIC 2017 dataset, the LBP extractor obtained the best overall results with Spe 90.16%, Sen 88%, Ppv 89.37%, *F* score 88.08%, Hm 88.06% and Acc 88% with the MLP classifier as shown in [Table 5](#).

The HU Moments also obtained a relevant result very close to the LBP with 91.69%, 87.04%, 90.14%, 87.58%, 88.06% and 87.4%, respectively. This data points out that the lesions present in the ISIC 2017 dataset have characteristics more related to their size and color

throughout their region.

The SCM applied to the ISIC 2017 dataset has results generally lower than the previous analysis. However, the application of the SCM in the frequency domain with the linear LSSVM classifier, shown in [Table 6](#), reaches a better value than the others with general metrics of Spe 92.15%, Sen 89.93%, Ppv 91.29%, *F* score 90%, Hm 90.54% and Acc 89.93%.

Again, the results with the Gaussian and Laplace filters have very close values, indicating that the melanoma in this dataset is equally identified by both the low and high frequencies, thus reinforcing the importance of the application of band-pass filters.

Among the analyses by [Tables 1–6](#), one can see that SCM with frequency domain contemplates all main features that characterize the skin lesion but, unlike LBP, GLCM, and HU, the SCM works in all datasets with the same discriminant power when configured with the frequency domain approach.

By analyzing the other SCM configuration using the Gaussian, Sobel and Laplace filters, the proposed approach is working as a band-pass filter making it consider multiple patterns in the image.

This work also compared the proposed method with different up-to-date methods applied to the same datasets. [Table 7](#) shows the Sen, Spe, Acc, and AUC of each method. The proposed results were taken from [Tables 2, 4 and 6](#). The AUC metric was calculated by averaging the results obtained in each of the datasets after cross-validation.

For the PH2 dataset, the methodology proposed in this work had the best results with Sen 99.4%, Spe 99.2%, Acc 99% and AUC 99%. The high values presented are justified, because, in addition to the robustness of the SCM, the PH2 dataset has more uniform images, thus fails to identify different patterns.

Using the same dataset, [Satheesha et al. \(2017\)](#) propose a 3d skin lesion reconstruction method to classify the dermoscopy images using both depth and 3-D shape as main features. [Bi et al. \(2016\)](#) propose a method based on multi-scale lesion-biased representation and joint reverse classification.

A important point of divergence between Satheesha et al. (2017), Bi et al. (2016), and the proposed approach is in preprocessing mainly in the contrast adjustment of the lesion. In the paper presented by Waheed et al. (2017) even with contrast adjustment, the use of color and texture features seen to be not enough to discriminate the normal from melanoma lesion.

The application of the SCM in the ISIC 2016 dataset also obtained, except Spe, the best values among the methods presented with Sen 95.23%, Spe 94.57%, Acc 94.5%, and AUC 92%. Spe obtained a value similar to that presented by Yu et al. (2017a). In addition of the contrast normalization, the proposed method also has a important discriminative characteristic, but different of Yu et al. (2017a,b) and Lopez et al. (2017) that uses spatial domain analysis with the CNN, the proposed method work extract the main structural properties from both frequency domain and spatial domain. Despite the impact generated by the variation of noise present in the ISIC 2016 dataset, the proposed method managed to obtain a balanced rate in its classification.

In the ISIC 2017 dataset, the proposed method obtained Sen 92.15%, Spe 89.9%, Acc 89.9% and AUC 89%. The SCM presented better values than the other methods for Sen and Acc. Note: however, the SCM, in general, obtained a better classification balance when associated with Sen and Spe together. As well as ISIC 2016 compared methods, Matsunaga et al. (2017), Sousa and de Moraes (2017) and Li and Shen (2017) use the CNN as the main tool. This could indicate that existing structural information that is better shown with frequency analysis.

#### 4. Conclusion and future work

This work proposes an innovation in the configuration of the SCM for automatic classification of skin lesions by using the frequency domain analysis.

The advantage of the combination between SCM and frequency domain lies in the ability to dynamically improve image structural characteristics, reflecting in the better discrimination of the data. The results show that the SCM reached more expressive and expressive values in all the databases, even when compared to the existing methods in the literature.

In addition to reinforcing the efficiency of the current ABCD technique used by specialists, this work also showed the possibility of a very relevant computational model in which its behavior is strongly assimilated to that technique and, therefore, an important tool to be included in systems to aid clinical diagnoses by taking into account the same characteristics. As a future work, the intention is to validate this method in other databases as well as the inclusion of new models for application and analysis in dermoscopy images.

#### References

- Almaraz-Damian, J., Ponomaryov, V., Rendon-Gonzalez, E., 2016. Melanoma CADe based on ABCD rule and haralick texture features. In: 2016 9th International Kharkiv Symposium on Physics and Engineering of Microwaves, Millimeter and Submillimeter Waves (MSMW). IEEE. pp. 1–4.
- Bi, L., Kim, J., Ahn, E., Feng, D., Fulham, M., 2016. Automatic melanoma detection via multi-scale lesion-biased representation and joint reverse classification. 2016 IEEE 13th International Symposium on Biomedical Imaging (ISBI) 1055–1058. <http://dx.doi.org/10.1109/ISBI.2016.7493447>.
- Codella, N.C., Gutman, D., Celebi, M.E., Helba, B., Marchetti, M.A., Dusza, S.W., et al., 2017. Skin lesion analysis toward melanoma detection: a challenge at the 2017 international symposium on biomedical imaging (ISBI), hosted by the international skin imaging collaboration (ISIC). [arXiv:1710.05006](https://arxiv.org/abs/1710.05006).
- de Souza, A.H., Corona, F., Barreto, G.A., Miche, Y., Lendasse, A., 2015. Minimal learning machine: a novel supervised distance-based approach for regression and classification. Neurocomputing 164, 34–44.
- de Souza, J.W., Almeida, J.S., Rebouças Filho, P.P., 2017. A new approach for the diagnosis of Parkinson's disease using a similarity feature extractor. In: International Conference on Intelligent Systems Design and Applications. Springer. pp. 21–31.
- de Souza, J.W., Alves, S.S., Rebouças, E.D.S., Almeida, J.S., Rebouças Filho, P.P., 2018. A new approach to diagnose Parkinson's disease using a structural cooccurrence matrix for a similarity analysis. Comput. Intell. Neurosci. 2018.
- Demyanov, S., Chakravorty, R., Abedini, M., Halpern, A., Garnavi, R., 2016. Classification of dermoscopy patterns using deep convolutional neural networks. In: 2016 IEEE 13th International Symposium on Biomedical Imaging (ISBI). IEEE. pp. 364–368.
- Fisher, R., Perkins, S., Walker, A., Wolfart, E., 1994. Hypermedia Image Processing Reference. Department of Artificial Intelligence, University of Edinburgh.
- Ge, Z., Demyanov, S., Bozorgtabar, B., Abedini, M., Chakravorty, R., Bowling, A., et al., 2017. Exploiting local and generic features for accurate skin lesions classification using clinical and dermoscopy imaging. In: 2017 IEEE 14th International Symposium on Biomedical Imaging (ISBI 2017). IEEE. pp. 986–990.
- Gu, Y., Zhou, J., Qian, B., 2017. Melanoma detection based on Mahalanobis distance learning and constrained graph regularized nonnegative matrix factorization. In: 2017 IEEE Winter Conference on Applications of Computer Vision (WACV). IEEE. pp. 797–805.
- Gutman, D., Codella, N.C., Celebi, E., Helba, B., Marchetti, M., Mishra, N., et al., 2016. Skin lesion analysis toward melanoma detection: a challenge at the international symposium on biomedical imaging (ISBI) 2016, hosted by the international skin imaging collaboration (ISIC). [arXiv:160501397](https://arxiv.org/abs/160501397).
- Haralick, R.M., Shanmugam, K., et al., 1973. Textural features for image classification. IEEE Trans. Syst. Man Cybern. 3 (6), 610–621.
- Haykin, S.S., 2009. Neural Networks and Learning Machines, vol.3 Pearson Upper Saddle River, NJ, USA.
- Holanda, G.B., Souza, J.W.M., Lima, D.A., Marinho, L.B., Girão, A.M., Bezerra Frota, J.B., Rebouças Filho, P.P., 2018. Development of OCR system on android platforms to aid reading with a refreshable Braille display in real time. Measurement 120, 150–168.
- Hu, M.K., 1962. Visual pattern recognition by moment invariants. IRE Trans. Inf. Theory 8 (2), 179–187.
- Kasmi, R., Mokrani, K., 2016. Classification of malignant melanoma and benign skin lesions: implementation of automatic ABCD rule. IET Image Process. 10 (6), 448–455.
- Kavitha, J., Suruliandi, A., 2016. Texture and color feature extraction for classification of melanoma using SVM. In: International Conference on Computing Technologies and Intelligent Data Engineering (ICCTIDE). IEEE. pp. 1–6.
- Kavya, S., Saranya, S., 2016. Routine identification of melanoma disease using global and local features. In: 2016 International Conference on Computer Communication and Informatics (ICCCI). IEEE. pp. 1–4.
- Li, Y., Shen, L., 2017. Skin lesion analysis towards melanoma detection using deep learning network. [arXiv:170300577](https://arxiv.org/abs/170300577).
- Lopez, A.R., Giro-i Nieto, X., Burdick, J., Marques, O., 2017. Skin lesion classification from dermoscopic images using deep learning techniques. In: 2017 13th IASTED International Conference on Biomedical Engineering (BioMed). IEEE. pp. 49–54.
- Marinho, L.B., de Souza Junior, A., Rebouças Filho, P.P., 2016. A new approach to human activity recognition using machine learning techniques. In: International Conference on Intelligent Systems Design and Applications. Springer. pp. 529–538.
- Marinho, L.B., Almeida, J., Mendes de Souza, J.W., Albuquerque, V.H.C., Rebouças Filho, P.P., 2017. A novel mobile robot localization approach based on topological maps using classification with reject option in omnidirectional images. Expert Syst. Appl. 72, 1–17.
- Marinho, L.B., Rebouças Filho, P.P., Almeida, J.S., Souza, J.W.M., Souza Junior, A.H., de Albuquerque, V.H.C., 2018. A novel mobile robot localization approach based on classification with rejection option using computer vision. Comput. Electr. Eng. 68, 26–43.
- Matsunaga, K., Hamada, A., Minagawa, A., Koga, H., 2017. Image classification of melanoma, nevus and seborrheic keratosis by deep neural network ensemble. [arXiv:170303108](https://arxiv.org/abs/170303108).
- Mendonça, T., Ferreira, P.M., Marques, J.S., Marcal, A.R., Rozeira, J., 2013. PH2 – a dermoscopic image database for research and benchmarking. In: 2013 35th Annual International Conference of the IEEE Engineering in Medicine and Biology Society (EMBC). IEEE. pp. 5437–5440.
- Mesquita, D.P.P., Gomes, J.P.P., Junior, A.H.S., 2015. Ensemble of minimal learning machines for pattern classification. In: International Work-Conference on Artificial Neural Networks. Springer. pp. 142–152.
- Mete, M., Sirakov, N.M., Griffin, J., Menter, A., 2016. A novel classification system for dysplastic nevus and malignant melanoma. In: 2016 IEEE International Conference on Image Processing (ICIP). IEEE. pp. 3414–3418.
- Neto, E.C., Gomes, S.L., Rebouças Filho, P.P., de Albuquerque, V.H.C., 2015. Brazilian vehicle identification using a new embedded plate recognition system. Measurement 70, 36–46.
- Ojala, T., Pietikainen, M., Harwood, D., 1994. Performance evaluation of texture measures with classification based on kullback discrimination of distributions. In: Proceedings of the 12th IAPR International Conference on Pattern Recognition, 1994. Vol. 1 – Conference A: Computer Vision & Image Processing. IEEE. pp. 582–585.
- Rahman, M., Alpaslan, N., Bhattacharya, P., 2016. Developing a retrieval based diagnostic aid for automated melanoma recognition of dermoscopic images. In: 2016 IEEE Applied Imagery Pattern Recognition Workshop (AIPR). IEEE. pp. 1–7.
- Ramalho, G.L.B., Rebouças Filho, P.P., Medeiros, F.N.S.d., Cortez, P.C., 2014a. Lung disease detection using feature extraction and extreme learning machine. Rev. Bras. Eng. Bioméd. 30 (3), 207–214.
- Ramalho, G.L.B., Rebouças Filho, P.P., Medeiros, F.N.S.d., Cortez, P.C., 2014b. Lung disease detection using feature extraction and extreme learning machine. Rev. Bras. Eng. Bioméd. 30 (3), 207–214.
- Ramalho, G.L.B., Ferreira, D.S., Rebouças Filho, P.P., de Medeiros, F.N.S., 2016. Rotation-invariant feature extraction using a structural co-occurrence matrix. Measurement 94, 406–415.
- Rebouças Filho, P.P., Cortez, P.C., Da Silva Barros, A.C., De Albuquerque, V.H.C., 2014. Novel adaptive balloon active contour method based on internal force for image segmentation – a systematic evaluation on synthetic and real images. Expert Syst. Appl. 41 (17), 7707–7721.
- Rebouças Filho, P.P., Cortez, P.C., da Silva Barros, A.C., Albuquerque, V.H.C., Tavares,

- J.M.R., 2017a. Novel and powerful 3d adaptive crisp active contour method applied in the segmentation of CT lung images. *Med. Image Anal.* 35, 503–516.
- Rebouças Filho, P.P., da Silva Barros, A.C., Ramalho, G.L., Pereira, C.R., Papa, J.P., de Albuquerque, V.H.C., 2017b. Automated recognition of lung diseases in CT images based on the optimum-path forest classifier. *Neural Comput. Appl.* 1–14.
- Rebouças Filho, P.P., Sarmento, R.M., Holanda, G.B., de Alencar Lima, D., 2017c. New approach to detect and classify stroke in skull ct images via analysis of brain tissue densities. *Comput. Methods Programs Biomed.* 148, 27–43.
- Rebouças Filho, P.P., Rebouças, E.d.S., Marinho, L.B., Sarmento, R.M., Tavares, J.M.R., de Albuquerque, V.H.C., 2017d. Analysis of human tissue densities: a new approach to extract features from medical images. *Pattern Recognit. Lett.* 94, 211–218.
- Rodrigues, M.B., Marinho, L.B., Nóbrega, R.V.M., Souza, J.W.M., Rebouças Filho, P.P., 2016. Lung segmentation in chest computerized tomography images using the border following algorithm. In: International Conference on Intelligent Systems Design and Applications. Springer. pp. 539–548.
- Rodrigues, M.B., Da Nóbrega, R.V.M., Alves, S.S.A., Rebouças Filho, P.P., Duarte, J.B.F., Sangaiah, A.K., et al., 2018. Health of things algorithms for malignancy level classification of lung nodules. *IEEE Access* 6, 18592–18601.
- Sabbaghi, S., Aldeen, M., Garnavi, R., 2016. A deep bag-of-features model for the classification of melanomas in dermoscopy images. In: 2016 IEEE 38th Annual International Conference of the Engineering in Medicine and Biology Society (EMBC). IEEE. pp. 1369–1372.
- Samui, P., Kothari, D., 2011. Utilization of a least square support vector machine (LSSVM) for slope stability analysis. *Sci. Iran.* 18 (1), 53–58.
- Satheesha, T., Satyanarayana, D., Prasad, M.G., Dhruve, K.D., 2017. Melanoma is skin deep: a 3d reconstruction technique for computerized dermoscopic skin lesion classification. *IEEE J. Transl. Eng. Health Med.* 5, 1–17.
- Skin Cancer Foundation SCF, 2015. Skin Statistics. <https://www.cdc.gov/stroke/facts.htm>.
- Song, F., Chen, S.T., Li, X., Han, J., 2018. Personal history of keratinocyte carcinoma is associated with reduced risk of death from invasive melanoma in men. *J. Am. Acad. Dermatol.*
- Sousa, R.T., de Moraes, L.V., 2017. Araguaia medical vision lab at isic 2017 skin lesion classification challenge. [arXiv:1703.00856](https://arxiv.org/abs/1703.00856).
- Vapnik, V.N., Vapnik, V., 1998. Statistical Learning Theory, vol. 1 Wiley, New York.
- Waheed, Z., Waheed, A., Zafar, M., Riaz, F., 2017. An efficient machine learning approach for the detection of melanoma using dermoscopic images. In: International Conference on Communication, Computing and Digital Systems (C-CODE). IEEE. pp. 316–319.
- Yu, L., Chen, H., Dou, Q., Qin, J., Heng, P.A., 2017a. Automated melanoma recognition in dermoscopy images via very deep residual networks. *IEEE Trans. Med. Imaging* 36 (4), 994–1004.
- Yu, Z., Ni, D., Chen, S., Qin, J., Li, S., Wang, T., et al., 2017b. Hybrid dermoscopy image classification framework based on deep convolutional neural network and fisher vector. In: 2017 IEEE 14th International Symposium on Biomedical Imaging (ISBI 2017). IEEE. pp. 301–304.